Journal of Biomolecular NMR, 8 (1996) 453–476
ESCOM



J-Bio NMR 392

# Investigations of peptide hydration using NMR and molecular dynamics simulations: A study of effects of water on the conformation and dynamics of antamanide

Jeffrey W. Peng*, Celia A. Schiffer**, Ping Xu***,
Wilfred F. van Gunsteren**** and Richard R. Ernst****

*Laboratorium für Physikalische Chemie, ETH-Zentrum, Universitätsstrasse 22, CH-8092 Zürich, Switzerland*

Received 2 July 1996
Accepted 28 August 1996

*Keywords:* Hydration; Computer simulation; Dynamics; Antamanide; Relaxation; Molecular dynamics

**Summary**

The influence of water binding on the conformational dynamics of the cyclic decapeptide antamanide dissolved in the model lipophilic environment chloroform is investigated by NMR relaxation measurements. The water–peptide complex has a lifetime of 35 μs at 250 K, which is longer than typical lifetimes of water–peptide complexes reported in aqueous solution. In addition, there is a rapid intracomplex mobility that probably involves librational motions of the bound water or water molecules hopping between different binding sites. Water binding restricts the flexibility of antamanide. The experimental findings are compared with GROMOS molecular dynamics simulations of antamanide with up to eight bound water molecules. Within the simulation time of 600 ps, no water molecule leaves the complex. Additionally, the simulations show a reduced flexibility for the complex in comparison with uncomplexed antamanide. Thus, there is a qualitative agreement between the experimental NMR results and the computer simulations.

## Introduction

Molecular interaction and recognition occur in both aqueous and lipophilic environments. In both media, the binding of water can be important for the structure and activity of a biomolecule or drug. In this paper, we focus on the interaction of an ion carrier peptide with water molecules in a model lipophilic environment by combining nuclear magnetic resonance studies with molecular dynamics (MD) simulations. The selected model system, antamanide (cyclo-Val-Pro-Pro-Ala-Phe-Phe-Pro-Pro-Phe-Phe), acts as a carrier for sodium, thallium and calcium ions (Wieland et al., 1972) and has water-binding properties (Karle et al., 1979). Chloroform is often used as a simple model for a lipophilic environment. Antamanide is conformationally constrained and yet possesses multiple backbone conformations that interconvert rapidly in solution (Patel, 1973; Kessler et al., 1988; Blackledge et al., 1993). It is an antidote against toxins native to the mushroom *Amanita phalloides* (Wieland and Faulstich, 1978).

Earlier X-ray diffraction studies have revealed eight water molecules per antamanide molecule in the single crystal, four of which are bound in the interior of the peptide ring (Karle et al., 1979). It was suggested that these water molecules stabilize the peptide backbone by

*Present address: Vertex Pharmaceuticals Inc., 130 Waverly Street, Cambridge, MA 02139-4242, U.S.A.
**Present address: Department of Protein Engineering, Genentech, Inc., 460 Point San Bruno Boulevard, South San Francisco, CA 94080, U.S.A.
***Present address: Biotechnology Research Institute, National Research Council Canada, 6100 Royalmount Avenue, Montreal, PQ, Canada H4P 2R2.
****To whom correspondence should be addressed.

*Supplementary Material:* Five tables containing listings of $H^N$, $H^\alpha$, and $C^\alpha$ chemical shifts for both water-free and water-containing antamanide samples (Tables S1a,b), a comparison of NOE-derived interproton distances from the two samples (Table S2), $^{13}C^\alpha$ $R_1$, $R_2$, and NOE values for both samples (Tables S3a,b,c), $S^2$ and $R_{ex}$ values for both samples (Table S4), and a comparison of NOE-derived interproton distances with those derived from the GROMOS molecular dynamics simulations (Table S5) are available on request from the authors.

cross-ring hydrogen bonds. Here, we investigate the influence of these water molecules on the conformational dynamics of antamanide in chloroform solution. This involves studying how the conformational equilibrium and the flexibility of antamanide are affected by the presence of small amounts of water in nonaqueous solution, and characterizing the water exchange dynamics.

NMR experiments include two-dimensional nuclear Overhauser spectroscopy (2D NOESY) to assess the effects of the water molecules upon the peptide conformation, and to estimate the residence time of complexed water molecules. Backbone flexibility is examined through measurements of proton rotating-frame and $^{13}C^{\alpha}$ laboratory-frame relaxation rate constants. To complement the NMR experiments, MD simulations have been performed on the antamanide–water system in a chloroform bath. The simulations start from the crystal structure (Karle et al., 1979) using various numbers of water molecules. The duration of the simulations is between 100 ps and 1 ns. This implies that a single simulation trajectory cannot visit all relevant low-energy backbone water-binding conformations, especially those separated by relatively high energy barriers. In an effort to reduce this problem, we have performed a set of MD simulations with varying initial conditions. The set of simulations permits the sampling of multiple low-energy conformations. Analysis of the simulations may help interpret the experimental observations.

## Methods

*Antamanide sample preparation*

Antamanide samples with varying amounts of water were prepared in the laboratory of Prof. H.H. Limbach at the Freie Universität in Berlin, Germany. All samples consisted of 10 mg of antamanide dissolved in 500 µl of deuterated chloroform ($CDCl_3$), resulting in a concentration of 17.4 mM. Two samples were selected for our study: a water-free sample, and a sample having a 3:1 molar ratio of water to antamanide. Henceforth, these samples will be referred to as the water-free and water-containing samples.

We experienced considerable difficulties in maintaining an equilibrated sample system of chloroform, water, and antamanide during the NMR experiments. At elevated temperatures (≥ 300 K), water started to fractionate and moved almost quantitatively to the (slightly colder) top of the sealed sample tube. This led to the disappearance of the water proton signal. At temperatures below 260 K, the saturated equilibrium solution contained an antamanide–$(H_2O)_n$ complex with $n \leq 2$. The surplus water was freezing out. The low solubility of water in chloroform led to long equilibration times of several hours.

*NMR spectroscopy*

All NMR experiments were performed on a Bruker AMX-600 spectrometer. The experiments included 2D NOESY spectra (Kumar et al., 1981), proton rotating-frame longitudinal relaxation rate ($R_{1\rho}$) measurements (Redfield, 1955), and inverse-detected $^{13}C^{\alpha}$ relaxation rate determinations (Kay et al., 1987; Sklenář et al., 1987; Nirmala and Wagner, 1988).

NOESY spectra were acquired at 250 K for the water-free and the water-containing samples. The data sets consisted of 1024 FIDs, each containing 2048 complex $t_2$ points. The mixing time was 150 ms, a value that lies within the initial rate regime of the intramolecular NOE cross-peak buildup (Blackledge et al., 1993). For each $t_1$ value, 16 scans were recorded with an inter-scan delay of 3.5 s. The TPPI technique provided sign discrimination of the $\omega_1$ frequencies (Marion and Wüthrich, 1983). The sweep widths were 5814 Hz for all NOESY spectra. All data were processed using Bruker UXNMR software. Prior to Fourier transformation, the FIDs were multiplied with sine-squared functions, phase-shifted by 60°. The final matrix sizes consisted of 1024 × 1024 real points. NOE cross peaks between protons i and j were integrated using FELIX 2.1 (Biosym Technologies, Inc., San Diego, CA, U.S.A.) to yield distances $d_{ij}$ via the relation

$$d_{ij} = d_{ref} (V_{ref} / V_{ij})^{1/6} \quad (1)$$

(Noggle and Schirmer, 1971). Equation 1 uses the NOE cross-peak volume $V_{ref}$ of a nuclear pair with a known reference distance, $d_{ref}$, to extract all other distances $d_{ij}$. The relation assumes that $d_{ref}$ belongs to a rigid fragment and that the correlation time of the isotropic molecular tumbling is the same for all internuclear vectors. The volume of the NOE cross peak corresponding to the $H^{\gamma}$-$H^{\gamma'}$ geminal pair of $Pro^8$ was chosen for $V_{ref}$, and $d_{ref}$ was set to 1.795 Å. The $Pro^8$ $\gamma\gamma'$ geminal pair was chosen for its well-resolved cross peak and its lack of significant internal mobility (Mádi et al., 1990). Uncertainties in the $d_{ij}$ distances were obtained through estimates of the cross-peak volume fluctuations. Specifically, two additional

*Abbreviations:* BPTI, basic pancreatic trypsin inhibitor; CPMG, Carr–Purcell–Meiboom–Gill; CSA, chemical shift anisotropy; CW, continuous wave; 1D, 2D, one-, two-dimensional; DD, dipole–dipole; DEPT, distortionless enhancement by polarization transfer; FID, free induction decay; GROMOS, Groningen Molecular Simulation package; kHz, kilohertz; MD, molecular dynamics; MEDUSA, multi-conformational evaluation of distance constraints using a stochastically constrained minimization algorithm; MHz, megahertz; NOE, nuclear Overhauser enhancement; NOESY, 2D cross-relaxation spectroscopy; rf, radio frequency; rmsd, root-mean-squared deviation; ROE, rotating frame Overhauser enhancement; SPC/E, extended simple point charge model; TPPI, time-proportional phase incrementation.

NOESY spectra (512 $t_1$ increments by 2048 $t_2$ points) were acquired for the water-containing sample under the same experimental conditions, and 14 interresidue cross peaks were integrated and compared. The average magnitude of the volume differences was $\delta V \approx 1\%$ of the $Pro^8$ $\gamma\gamma'$ reference cross-peak volume. This value was used to judge the reliability of the distance measurements. Upper and lower distance limits for pairs of nuclei i and j were then calculated using the relations

$$d_{ij,short} = d_{ref}\left(\frac{V_{ref}}{V_{ij} + \delta V}\right)^{1/6} - d_{extra} \qquad (2)$$

and

$$d_{ij,long} = d_{ref}\left(\frac{V_{ref}}{V_{ij} - \delta V}\right)^{1/6} + d_{extra} \qquad (3)$$

The $d_{extra}$ term in Eqs. 2 and 3 accounts for any further uncertainties in the distance calculations (vide infra).

Proton rotating-frame relaxation rate constants, $R_{1\rho}(H)$, were measured at 250 K using the sequence $90^\circ_x$-[Spin-Lock]$_y$-acquire (Blackledge et al., 1993). The initial 90° proton pulse creates proton transverse y magnetization, which is then spin-locked by on-resonance continuous-wave (CW) irradiation for a duration $T_{lock}$. For each of the backbone protons $Val^1$ $H^N$, $Pro^3$ $H^\alpha$, $Ala^4$ $H^N$, $Ala^4$ $H^\alpha$, $Phe^5$ $H^\alpha$, and $Phe^6$ $H^N$, a series of 12 FIDs was recorded with $T_{lock}$ = 10, 20, 20, 30, 40, 50, 60, 80, 100, 130, 130, and 160 ms for the water-free and for the water-containing samples. The FIDs were Fourier-transformed to yield proton peak intensities versus $T_{lock}$. The intensities were fitted to the two-parameter single-exponential decay, $I(T_{lock}) = A \exp(-R_{1\rho}T_{lock})$, to give $R_{1\rho}(H)$. The $R_{1\rho}(H)$ measurements were repeated at the rf field strengths 9.7, 6.5, 5.4, 3.9, 2.9, 2.4, and 1.2 kHz. The $R_{1\rho}(H)$ value of the water resonance was also measured, using the rf field strengths 11.4, 8.9, 7.4, 6.2, 4.5, 3.4, 2.8, 1.9, and 1.3 kHz.

$^{13}C^\alpha$ relaxation parameters including $R_1 = 1/T_1$, $R_2 = 1/T_2$, and the heteronuclear steady-state NOE were measured at 250 K for both antamanide samples at natural abundance. DEPT polarization enhancement (Doddrell et al., 1982) was used (except for the NOE measurements) together with inverse detection using a reverse DEPT (Kay et al., 1987; Sklenář et al., 1987; Nirmala and Wagner, 1988) in either 1D or 2D mode. The measurements of the longitudinal relaxation rate constant, $R_1 = 1/T_1$, employed the inversion-recovery technique. For each of the inter-pulse delays 10, 50, 50, 75, 100, 100, 125, 150, 200, 300, 400, 600, 1000, and 2000 ms, 1024 scans were acquired. Proton saturation was applied during the inter-pulse delay to ensure an exponential recovery and to suppress cross-relaxation mediated by cross-correlation between the $^{13}C$-$^1H$ dipole–dipole (DD) and the $^{13}C$ chemical shift anisotropy (CSA) relaxation mechanisms (Boyd et al., 1990). A train of 120° pulses separated by 5 ms delays was used for the saturation. The resonance intensity I versus relaxation delay T was fitted to the three-parameter expression $I(T) = B + A \exp(-R_1T)$.

Measurements of the transverse relaxation rate constant, $R_2 = 1/T_2$, were performed with the Carr–Purcell–Meiboom–Gill (CPMG) technique (Carr and Purcell, 1954; Meiboom and Gill, 1958). The carbon 180° pulses were 75 μs long and the delay between successive 180° pulses was 1 ms, thus ensuring that only the relaxation rate of in-phase coherence was measured (Peng et al., 1991; Kay et al., 1992). Modifications to the basic CPMG technique (Palmer et al., 1992) were used to suppress DD–CSA cross-correlation artifacts. For both samples, 10 proton-detected 2D spectra were collected employing CPMG trains applied for 8.8, 8.8, 17.6, 26.4, 35.2, 44, 61.6, 88, 132, and 176 ms. Each spectrum was computed from 64 $t_1$ increments and 2048 $t_2$ points. Per $t_1$ increment, 64 scans were taken. The carbon sweep width was 4700 Hz, and sign discrimination was again achieved using TPPI. The cross-peak intensity versus CPMG duration was then fitted to the same single exponential two-parameter expression used in the $R_{1\rho}$ experiments to yield $R_2$.

Steady-state $^{13}C$ NOEs were determined from a pair of inverse-detected DEPT 2D spectra in the presence and absence of proton saturation, yielding the integrated signal intensities $I_{sat}$ and $I_{eq}$, respectively. The NOE was computed according to $NOE = (I_{sat} - I_{eq})/I_{eq}$ (Noggle and Schirmer, 1971). The spectral acquisition parameters were the same as in the $R_2$ measurements, with the exception that 160 scans were acquired for each $t_1$ increment, owing to the lack of an initial polarization transfer. Proton saturation was obtained in the same manner as in the $R_1$ experiments for a duration of 2.5 s. The heteronuclear dipole–dipole cross-relaxation rate constant, $R_c$, is deduced from $R_1$ and NOE via the relation $R_c = (R_1)(NOE)(\gamma_C/\gamma_H)$.

The Levenburg–Marquardt algorithm was used (Marquardt, 1963; Press et al., 1988) for data fitting. The parameter errors were estimated from uncertainties in the measured peak intensities. The peak intensity uncertainties were evaluated in two ways. First, the root-mean-squared deviation (rmsd) between the experimental intensities and those resulting from the Levenburg–Marquardt fit was used (Kamath and Shriver, 1989). In a second method, the fluctuations of the experimental intensities from duplicate spectra were used. The method yielding the larger uncertainty was then used to generate 500 artificial data sets, following a Monte Carlo procedure (Kamath and Shriver, 1989; Palmer et al., 1991). The rmsd of the resulting ensemble of fitted rate constants was taken as an estimate of the error for each rate constant.

*Motional models*

The NMR auto- and cross-relaxation rate constants are linear combinations of spectral density functions of the various motional processes sampled at several frequencies. The use of motional models enables these spectral density functions to be expressed as analytical functions of the underlying dynamical parameters. Below we summarize the models applied in this study.

The proton NOESY cross-peak intensities in the initial rate regime are proportional to the homonuclear dipole–dipole cross-relaxation rate constants (Macura and Ernst, 1980). The cross-relaxation rate constant $\Gamma_{ij}^{NOE}$ between two protons i and j is given by:

$$\Gamma_{ij}^{NOE} = q_{ij} \, (6J_{ij} \, (2\omega_o) - J_{ij} \, (0)) \qquad (4)$$

$J_{ij}(\omega)$ is the spectral density function of the process that affects the vector $\mathbf{d}_{ij}$. The prefactor is $q_{ij} = (\mu_0/4\pi)^2\gamma^4\hbar^2/20d_{ij}^6$, and $\omega_o$ is the proton Larmor frequency. For a model in which $\mathbf{d}_{ij}$ tumbles isotropically in solution with a correlation time $\tau_{eff}$, $J_{ij}(\omega)$ has the Lorentzian form

$$J_{ij}(\omega) = \frac{2\tau_{eff}}{1+(\omega\tau_{eff})^2} \qquad (5)$$

Proton rotating-frame relaxation rate constants $R_{1\rho}(H)$ are determined by the contribution of the dipolar relaxation $R_{DD}$ and by the exchange contribution $R_{ex}(\omega_1)$, leading to the sum:

$$R_{1\rho}\,(H) = R_{DD} + R_{ex}(\omega_1) \qquad (6)$$

$R_{ex}(\omega_1)$ arises from the modulation of proton chemical shifts due to exchange processes; it contains a dependence on the rf field strength $\omega_1$ that provides the desired information on the exchange dynamics. We consider a model in which a proton exchanges between two states A and B with the fractional populations $p_A$ and $p_B$, the chemical difference $\Delta$ (in Hz), and the exchange time constant $\tau_{ex}$. Then, $R_{1\rho}(H)$ is determined by (Deverell et al., 1970):

$$R_{DD} = p_A R_{DDA} + p_B R_{DDB} \qquad (7)$$

and

$$R_{ex}(\omega_1) = \frac{4\pi^2 p_A p_B \Delta^2 \tau_{ex}}{1+(\omega_1\tau_{ex})^2} \qquad (8)$$

where $R_{DDA}$ and $R_{DDB}$ are the dipolar relaxation contributions of the two states. Equation 8 conforms to our experimental conditions, in which the spin-lock is applied on-resonance with the exchange-averaged shift. The $R_{1\rho}(H)$ measurements are most informative when the exchange time constant $\tau_{ex} \approx 1/\omega_1$. The informative rf field dependence in $R_{1\rho}$ disappears when (i) the chemical shift difference $\Delta$ is too small; (ii) the equilibrium is one-sided, $p_A p_B \ll 1$; (iii) the process is very slow, $\tau_{ex} \gg 1/\omega_1$; or (iv) the process is very fast, $\tau_{ex} \ll 1/\omega_1$. These facts must be kept in mind when interpreting $R_{1\rho}$ measurements. The Levenburg–Marquardt algorithm was used to optimize the parameters $R_{DD}$, $\tau_{ex}$, and $K = 4\pi^2 p_A p_B \Delta^2$. Note that it is not possible to separate the factors $p_A p_B$ and $\Delta$.

The relaxation rates of $^{13}C^{\alpha}$ nuclei (at natural abundance) are determined by the heteronuclear one-bond DD interaction and, to a lesser extent, by the CSA of $C^{\alpha}$. We have measured the $^{13}C^{\alpha}$ rate constants $R_1$, $R_2$, and $R_c$ for both antamanide samples. Their expressions in terms of the spectral density functions $J_{CH}(\omega)$ are (Abragam, 1961; Ernst et al., 1987):

$$\begin{aligned} R_1 = q_{CH} \{ & J_{CH}(\omega_H - \omega_C) + 3J_{CH}(\omega_C) \\ & + 6J_{CH}(\omega_H + \omega_C) \} + cJ_{CH}(\omega_C) \end{aligned} \qquad (9)$$

$$\begin{aligned} R_2 = \frac{q_{CH}}{2} \{ & 4J_{CH}(0) + J_{CH}(\omega_H - \omega_C) + 3J_{CH}(\omega_C) \\ & + 6J_{CH}(\omega_H) + 6J_{CH}(\omega_H + \omega_C) \} \\ & + c\left\{\tfrac{2}{3}J_{CH}(0) + \tfrac{1}{2}J_{CH}(\omega_C)\right\} + R_{ex} \end{aligned} \qquad (10)$$

$$R_c = q_{CH} \{ 6J_{CH}(\omega_H + \omega_C) - J_{CH}(\omega_H - \omega_C) \} \qquad (11)$$

In the expressions for $R_1$ and $R_2$, c is a constant related to the $C^{\alpha}$ chemical shielding anisotropy. The constant $q_{CH}$ is given by:

$$q_{CH} = \left(\frac{\mu_0}{4\pi}\right)^2 \frac{\gamma_H^2\gamma_C^2\hbar^2}{20d_{CH}^6} \qquad (12)$$

The cross-relaxation rate constant $R_c$ is not directly measured; rather, it is deduced from $R_1$ and the steady-state NOE through the relation $NOE = (R_c\gamma_H/R_1\gamma_C)$. The $R_{ex}$ term in Eq. 10 allows for the possibility of chemical exchange contributions. If we assume a two-site exchange model, then $R_{ex}$ is equal to $R_{ex}(\omega_1 = 0)$ as in Eq. 8. The spectral density function $J_{CH}(\omega)$ characterizes the orienta-

TABLE 1
MOLECULAR DYNAMICS EQUILIBRATION PROTOCOL

| Procedure | Time (ps) | Temperature (K) | $k^{s}$ [a] (kJ/mol/Å$^2$) |
|---|---|---|---|
| Energy minimization | 500 steps | | 9999 |
| MD | 2.5 | 50 | 9000 |
| MD | 2.5 | 150 | 9000 |
| MD | 5.0 | 250 | 9000 |
| MD | 5.0 | 250 | 900 |
| MD | 5.0 | 250 | 100 |

[a] $k^s$ is the force constant for one peptide and the water molecules used in the harmonic positional restraining of the initial conformation of antamanide.

tional fluctuations of the $^{13}C^{\alpha}$-$H^{\alpha}$ bond and is analyzed using the approach of Lipari and Szabo (1982a,b). In its simplest form, this approach assumes that the overall molecular tumbling of the biomolecule and the internal fluctuations of the $C^{\alpha}$-H bond are statistically independent. The overall molecular tumbling is assumed to be isotropic and is described by a single correlation time $\tau_{rot}$. The internal motion of each $C^{\alpha}$-$H^{\alpha}$ bond is described by an order parameter $S^2$ and an internal correlation time $\tau_i$. The model form of $J_{CH}(\omega)$ is then the weighted sum of two Lorentzians:

$$J_{CH}(\omega) = 2\left\{\frac{S^2\tau_{rot}}{1+(\omega\tau_{rot})^2} + \frac{(1-S^2)\,\tau_e}{1+(\omega\tau_e)^2}\right\} \qquad (13)$$

The effective correlation time $\tau_e$ is given by $\tau_{rot}\,\tau_i/(\tau_{rot}+\tau_i)$. The site-specific parameters $S^2$ and $\tau_i$ and the global parameter $\tau_{rot}$ are then fitted to the relaxation data. Additionally, $R_{ex}$ may be adjusted for each $C^{\alpha}$-$H^{\alpha}$ bond to include the effects of chemical exchange.

*Methods of simulation*

The MD simulations were performed with the GROMOS force field and simulation package (van Gunsteren and Berendsen, 1987). Water was modeled using the SPC/E model (Berendsen et al., 1987) and chloroform by an all-atom model (Dietz and Heinzinger, 1984,1985; Tironi and van Gunsteren, 1994). The nonbonded parameters for the interactions between chloroform and the peptide or water atoms were obtained by using the geometric mean of the self-interaction parameters, i.e., $C_{6ij} = (C_{6ii}\,C_{6jj})^{1/2}$. The combination rules for the water–water and water–peptide interactions were defined in the original models and the GROMOS force field, respectively. For the interaction between a neutral carbon and SPC/E water oxygen, a corrected value of $C_{12} = 793.3$ (kcal/mol $Å^{12})^{1/2}$ was used (Mark et al., 1994). The crystal structure of antamanide (Karle et al., 1979) served as the starting conformation. The starting positions for the water molecules were also taken from the crystal structure. The antamanide–water system was first surrounded by a box containing equilibrated chloroform, such that the closest packing distance of antamanide to chloroform was 2.39 Å, and 15.0 Å to a box face. In the different simulations, the number of chloroform molecules used to fill the periodic box varied from 394 to 396.

The chloroform environment was equilibrated following the protocol of Table 1. The system was gradually heated from 50 to 250 K with tight harmonic positional restraints on the peptide and the associated crystallographic water molecules. The initial velocities were taken from a Maxwellian distribution at 50 K. Covalent bond lengths were constrained using the SHAKE procedure (Ryckaert et al., 1977) with a relative tolerance of $10^{-4}$. The time increment used in the leap-frog integration scheme was 0.002 ps. A cutoff radius of 14.0 Å for the nonbonded interactions was used in conjunction with the pair list, which was updated every 10 time steps. The temperature of the system was maintained by coupling to a heat bath (Berendsen et al., 1984) with a coupling constant of 0.1 ps. Coordinates were saved from the simulation every 0.2 ps.

Six simulations were performed for antamanide in chloroform:

(i) 8 $H_2O$, 1 ns duration at 250 K with data analysis for the final 600 ps.

(ii) 0 $H_2O$, 1 ns duration at 250 K with 600 ps analysis.

(iii) 1 $H_2O$ (no. 12 in Fig. 8a), 400 ps duration at 250 K with 300 ps analysis.

(iv) 1 $H_2O$ (no. 13 in Fig. 8a), 400 ps duration at 250 K with 300 ps analysis.

(v) 2 $H_2O$ most tightly nested within the peptide ring (nos. 12 and 13 in Fig. 8a), 400 ps duration at 250 K with 300 ps analysis.

(vi) 8 $H_2O$, 400 ps continuation of (i) at 290 K with 300 ps analysis for a test of the stability of the water network.

For each simulation, the rms fluctuations of the backbone dihedral angles were calculated. For dihedral angles showing a large fluctuation, which indicates a dihedral angle transition, the angles were analyzed as a function of time. For simulations (i) and (ii), the proline ring puckerings were also analyzed as a function of time to enable a comparison between the current simulations and those performed previously (Brüschweiler et al., 1992; Brunne et al., 1993; Schmidt et al., 1993), which used mean-force models for chloroform. The hydrogen bonding of antamanide to itself and to the complexed water molecules was analyzed in terms of the percentage of time a particular hydrogen bond exists. Hydrogen bonds were recognized by a distance between the hydrogen and the acceptor atom less than 2.5 Å, and a donor–hydrogen–acceptor angle greater than 135°.

## Results

*The NMR study*

*General behavior of the antamanide–water system*

The water proton chemical shift in the absence and presence of antamanide at 250 K gives a first indication of interactions between water molecules and antamanide. Water molecules alone in chloroform yield a resonance at $\delta_{free} = 1.64$ ppm. The addition of antamanide induces a downfield shift to $\delta_{obs} = 2.804$ ppm. Only a single water resonance can be detected. The area of the water resonance in the presence of antamanide is 3.7 times that of an isolated α-proton from antamanide. Accordingly, the water-containing sample has 1.84 water molecules per antamanide in solution at 250 K. However, a 1D proton

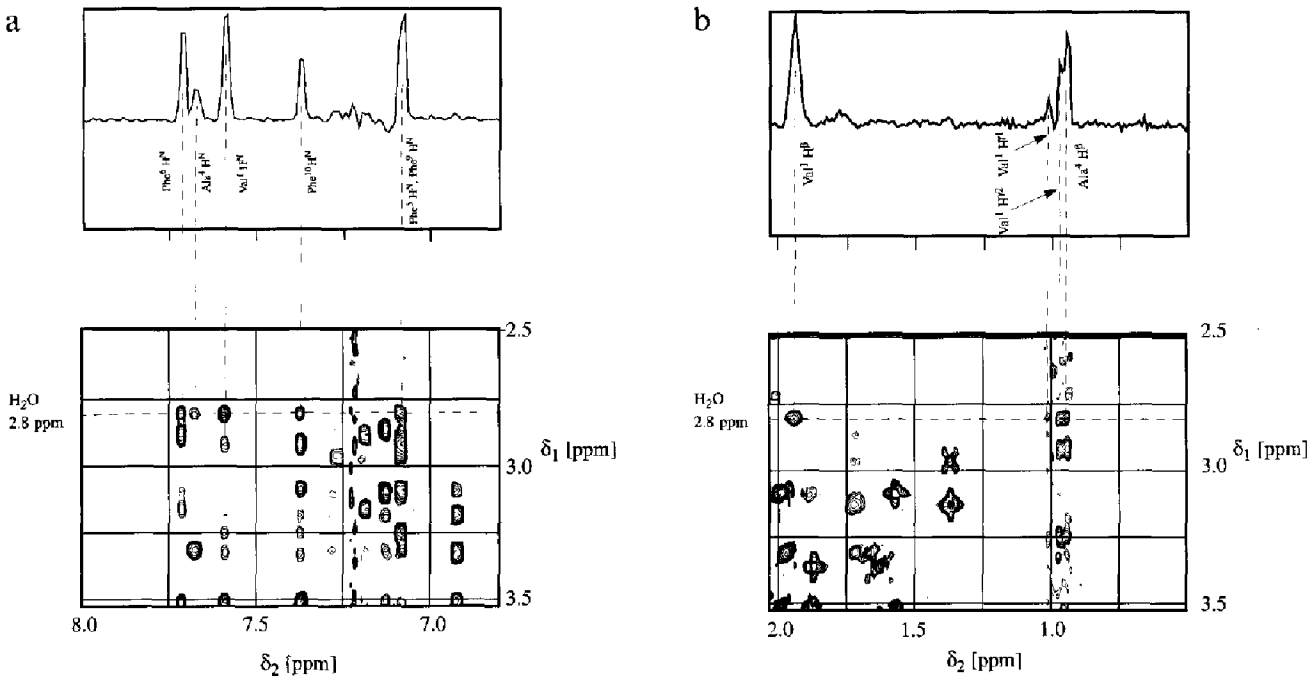


Fig. 1. Regions of a proton NOESY spectrum of water-containing antamanide in $CDCl_3$ at 600 MHz and T = 250 K. (a) The region containing intermolecular cross peaks between water and the amide protons. (b) Regions with cross peaks between water and the $Val^1$ β proton, and methyl protons of $Val^1$ and $Ala^4$. One-dimensional slices at the water resonance ($\delta_1 = 2.804$ ppm) are shown above the corresponding 2D regions. The mixing time was 150 ms.

NMR spectrum of the same sample at 293 K reveals a water resonance 5.7 times the area of a single α-proton resonance. Thus, there are 2.85 water molecules per antamanide in the sample. The fact that only 60% of the water is observable at 250 K suggests that the remaining water is frozen out.

At 250 K, the saturation concentration of water in chloroform is 0.006% by weight (Gibby and Hall, 1931). With the present antamanide concentration, this corresponds to 0.34 water molecules per antamanide, and the amount of complexed water is 1.5 water molecules per antamanide molecule. The fractional populations of complexed and free water are therefore $p_{bound} = 0.82$ and $p_{free} = 0.18$, respectively. The crystal structure of Karle et al. (1979) suggests that numerous binding configurations coexist for the 1.5 water molecules. The existence of a single water resonance implies that the water molecules exchange rapidly among the different environments. The chemical shift of bound water is then computed to be $\delta_{bound} = 3.06$ ppm, and the frequency change upon binding is $\nu_o(\delta_{bound} - \delta_{free}) = 852$ Hz.

The interaction between antamanide and the water molecules also perturbs certain chemical shifts of antamanide itself. This is revealed in a comparison of $H^N$, $H^\alpha$, and $C^\alpha$ chemical shifts from the water-free and water-containing samples. These shift values are provided in Tables S1a,b of the Supplementary Material. The chemical shift perturbations pinpoint specific water–antamanide interactions. For example, in the water-containing sample, $Val^1$ $H^N$ and $Ala^4$ $H^N$ shifts change by +0.16 and −0.19 ppm, respectively, relative to the water-free sample. The other $H^N$ nuclei also experience shift changes, with magnitudes ranging from 0.03 to 0.08 ppm. It is well known that $H^N$ chemical shift values are strongly influenced by the hydrogen-bonding state of the $H^N$ (Wagner et al., 1983; Pastore and Saudek, 1990; Wishart et al., 1991; de Dios et al., 1993a,b). Thus, the $H^N$ shift changes could reflect the formation of new intermolecular hydrogen bonds with water, and the corresponding rearrangements of intramolecular hydrogen bonds in antamanide.

Additionally, a number of $C^\alpha$ shifts are affected by the introduction of water molecules. The most pronounced changes occur for the contiguous stretch of residues $Phe^9$ $C^\alpha$, $Phe^{10}$ $C^\alpha$, and $Val^1$ $C^\alpha$, with changes of −0.49, −0.53, and +0.70 ppm, respectively, relative to the water-free sample. $Pro^2$ $C^\alpha$, $Pro^3$ $C^\alpha$, and $Pro^8$ $C^\alpha$ show the smallest perturbations. Some of the attached $H^\alpha$ protons also exhibit significant shift changes. The largest change occurs for $Phe^5$ $H^\alpha$, which moves upfield by 0.16 ppm upon the introduction of water. Thus, the residues experiencing the largest $C^\alpha$ shift perturbations are not necessarily the same as those experiencing the largest $H^\alpha$ shift perturbations. Recent theoretical and empirical studies have shown that the $C^\alpha$ and $H^\alpha$ shifts have a strong dependence on the local dihedral angles Φ, Ψ, and χ (Spera and Bax, 1991; Wishart et al., 1991; de Dios et al., 1993a,b). This dependence is stronger for the $C^\alpha$ nuclei than for the $H^\alpha$ nuclei, and the latter can also be influenced by non-

bonded environmental effects (e.g. magnetic anisotropy contributions from nearby carbonyl groups, ring current shifts). The $C^{\alpha}$ shift perturbations suggest an alteration of the antamanide backbone conformation due to the interaction with water molecules. However, the limited information contained in the chemical shifts does not allow deduction of specific backbone conformations. In addition, antamanide itself undergoes rapid conformational

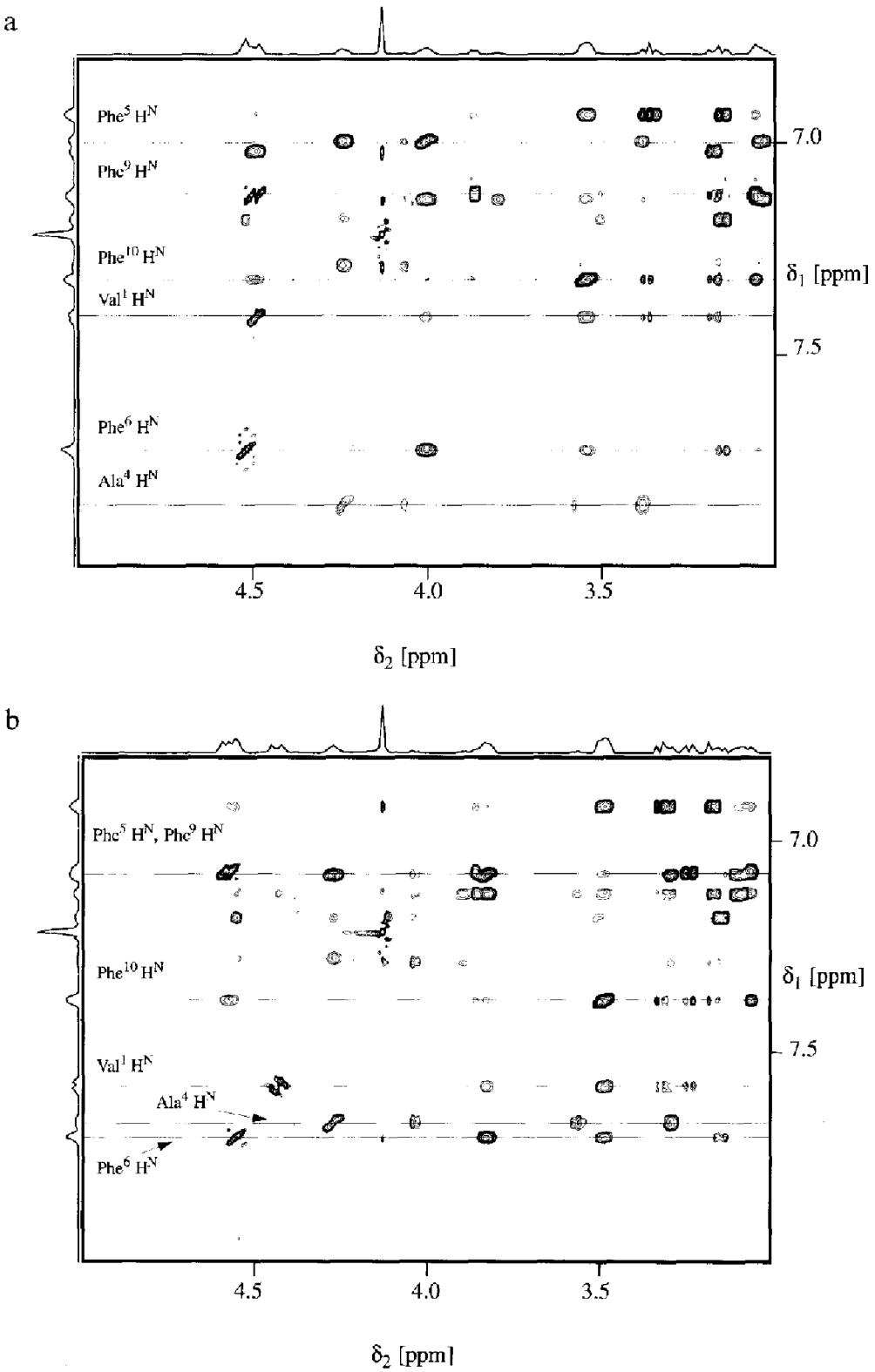


Fig. 2. $H^N/H^{\alpha}$ regions from NOESY spectra of (a) water-free antamanide and (b) water-containing antamanide. Both spectra were recorded at 600 MHz and T = 250 K for a mixing time of 150 ms. Only positive contours are shown.

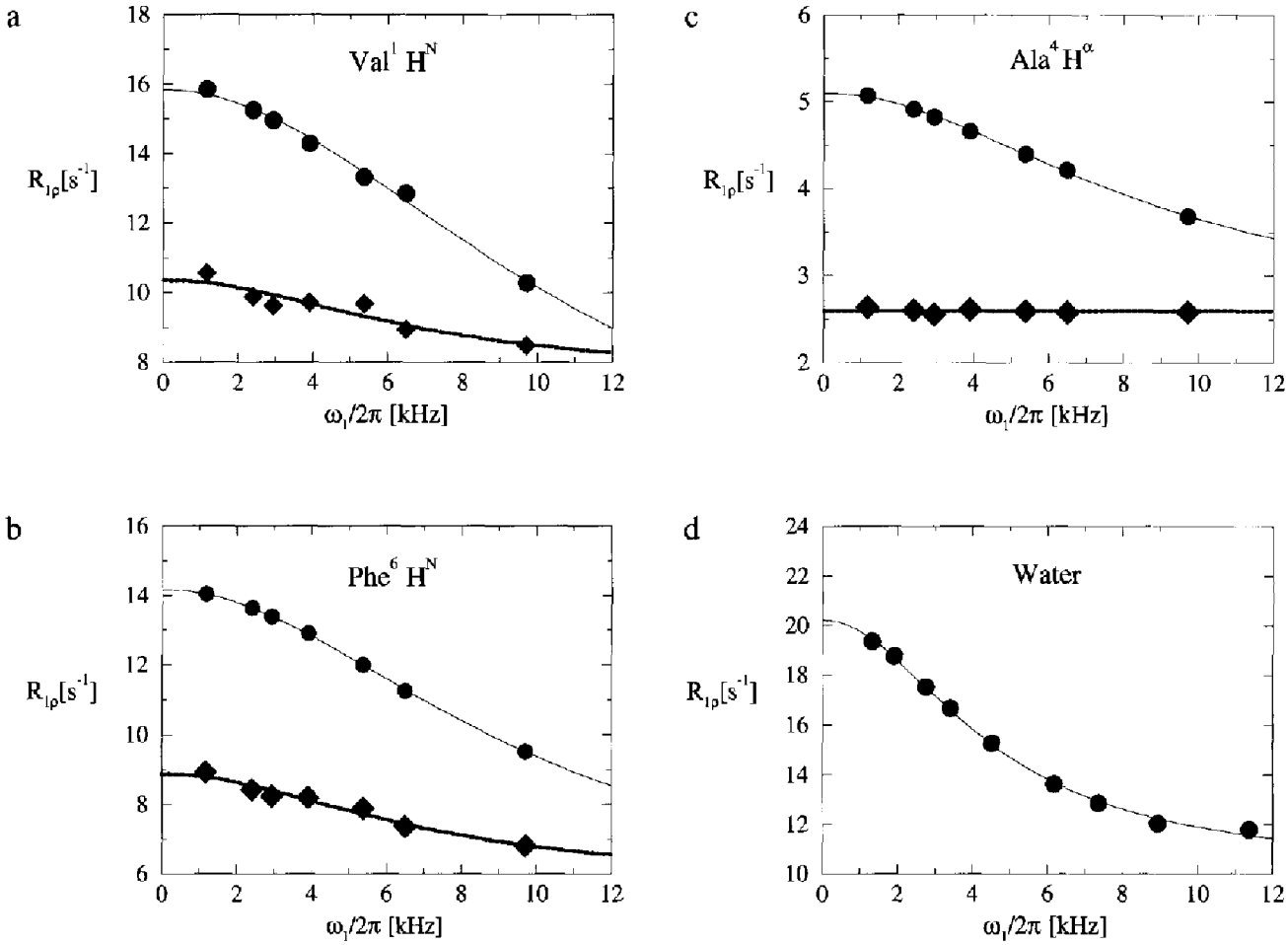


Fig. 3. Proton $R_{1\rho}$ relaxation-rate constants as a function of the spin-lock rf field strength $\omega_1/2\pi$ for three backbone protons and for water. The rates were measured at 250 K using a CW spin-lock. The filled circles denote $R_{1\rho}$ for water-free antamanide, while the diamonds denote $R_{1\rho}$ for water-containing antamanide. The lines are fits based on Eqs. 6–8 to the experimental values. (a) Val$^1$ H$^N$; (b) Phe$^6$ H$^N$; (c) Ala$^4$ H$^\alpha$; and (d) water resonance in the water-containing antamanide solution.

exchange (Burgermeister et al., 1974; Kessler et al., 1988; Blackledge et al., 1993), and the chemical shifts thus reflect the averaged structural properties of a dynamic ensemble of interconverting conformers.

*Cross-relaxation between water and antamanide*

At 250 K, intra- and intermolecular cross peaks in the NOESY spectra are positive with respect to the diagonal. The strongest intermolecular NOE cross peaks are those between water and the antamanide $H^N$ protons. ROESY spectra (Bothner-By et al., 1984), recorded under the same experimental conditions and with mixing times of 50 and 150 ms, show the same water–amide cross peaks, but inverted in sign with respect to the diagonal. This indicates that these intermolecular cross peaks are primarily a consequence of dipole–dipole cross-relaxation and not of chemical exchange (Otting and Wüthrich, 1989). The amide protons thus appear to be relevant hydration sites of antamanide. NOEs also exist between water and the side-chain β and γ protons of Val$^1$, and the β methyl protons of Ala$^4$. Figures 1a and b depict the water–antamanide NOE cross peaks for a NOESY experiment with a mixing time of 150 ms at the chemical shift of water $\delta_1 = 2.804$ ppm. The most intense NOEs are those involving Val$^1$ $H^N$ and Phe$^6$ $H^N$. Weaker NOEs are seen to the rest of the $H^N$ protons, and to the Val$^1$ side-chain resonances. The relative volumes of the $H^N$–water cross peaks, normalized to Val$^1$, are 1, 0.31, 0.61, 0.77, 0.61, and 0.51 for Val$^1$, Ala$^4$, Phe$^5$, Phe$^6$, Phe$^9$, and Phe$^{10}$, respectively.

At 271 K, all water–antamanide NOE cross peaks vanish. They reappear at 293 K, but with negative intensity with respect to the positive diagonal. The vanishing of the water–antamanide NOE cross peaks at 271 K therefore represents the zero-crossing. This suggests that the effects of chemical exchange between the amide $H^N$ protons and the water protons are indeed negligible. $H^N$–water proton exchange would result in a higher zero-crossing temperature for the $H^N$ protons than for the Val$^1$ and Ala$^4$ aliphatic protons, and a measurable disparity in cross-peak intensity between the $H^N$ protons versus the aliphatic protons at 293 K. Such effects are not observed.

While the $H^N$–water NOE cross peaks vanish at 271 K,

the cross peaks connecting the backbone protons of antamanide remain positive. This implies intra-complex mobility of the $H^N$–water proton–proton vectors, in addition to the overall molecular tumbling. This mobility could involve local water dynamics in the bound state, e.g. a rotation about a hydrogen bond, or an exchange process between different binding sites; this is discussed in further detail below.

*Comparison of NOE-derived distances between the water-free and water-containing samples*

To further assess the effect of water on the conformation of antamanide, we compare the $\tau_m = 150$ ms NOESY spectra for the water-free and water-containing samples at 250 K. Figure 2 shows excerpts from these spectra in the $H^N$-$H^\alpha$ region. The aforementioned chemical shift changes due to water binding, detailed in Tables S1a,b of the Supplementary Material, are obvious. Closer inspection of the two spectra reveals the same sets of NOE connectivities, and thus the spectra do not point to obvious conformational changes. Equations 1–3 were used to calculate a number of intramolecular proton–proton distances, $d_{ij}$, for the two samples, based on the integrated NOE cross-peak volumes. Differences between the distances $d_{ij,water\text{-}free}$ and $d_{ij,water\text{-}cont.}$ were considered significant only if they exceeded the range of fluctuations specified by $d_{ij,long}$ and $d_{ij,short}$ in Eqs. 2 and 3. The $d_{extra}$ term was set to 0.06 Å, which was the largest distance deviation observed in a comparison of 13 intraresidue distances for $Pro^3$ and $Pro^8$, which are assumed to be insensitive to water binding. A comparison of distances for 20 proton pairs is given in Table S2 of the Supplementary Material. For interresidue backbone–backbone distances, $d_{ij,water\text{-}cont.} < d_{ij,water\text{-}free}$. In contrast, the interresidue side-chain–side-chain distance $d_{\beta\beta}(9,4)$ shows $d_{ij,water\text{-}cont.} > d_{ij,water\text{-}free}$. Some of these changes can be rationalized by the MD simulations discussed below.

The changes in NOE intensities described above, along with the aforementioned $^{13}C^\alpha$ chemical shift perturbations, suggest that the multiconformational equilibrium of antamanide is perturbed by water binding. The identification of specific structural changes associated with this perturbation requires a detailed analysis of the NOE data using a multiconformational search algorithm, such as MEDUSA (Brüschweiler et al., 1991). At present, there is insufficient experimental data to successfully apply the MEDUSA algorithm. Specifically, this would also require homonuclear and heteronuclear vicinal coupling constants for the two samples, which have yet to be measured. Accordingly, a comparison of structure calculations for the water-free and water-containing samples is currently premature.

TABLE 2
WATER-FREE ANTAMANIDE $R_{1\rho}$ EXCHANGE PARAMETERS AT 250 K AND 600 MHz

| Proton | $\tau_{ex}$ (μs) | $\Delta_{app}$ (Hz)[a] | $R^*_{DD}$ ($s^{-1}$) |
|---|---|---|---|
| $Val^1$ $H^N$ | 14 | 304 | 2.94 |
| $Pro^3$ $H^\alpha$ | 17 | 119 | 3.36 |
| $Ala^4$ $H^N$ | 17 | 540 | 15.97 |
| $Ala^4$ $H^\alpha$ | 18 | 119 | 2.56 |
| $Phe^5$ $H^\alpha$ | 27 | 219 | 12.66 |
| $Phe^6$ $H^N$ | 16 | 240 | 4.86 |

[a] Assuming $p_A = p_B = 0.5$.

*Comparison of proton rotating-frame relaxation parameters*

We performed proton rotating-frame relaxation studies in order to investigate the influence of water binding on the peptide backbone dynamics at 250 K. $R_{1\rho}(H)$ rate constants at seven rf field strengths were determined for the $Val^1$ $H^N$, $Ala^4$ $H^\alpha$, $Ala^4$ $H^N$, $Phe^5$ $H^\alpha$, $Phe^6$ $H^N$, $Pro^3$ $H^\alpha$, and $Pro^8$ $H^\alpha$ of both samples. Figures 3a–d illustrate representative fits of the proton $R_{1\rho}(H)$ values by Eqs. 6–8 as functions of the applied rf field strength for three protons of both antamanide samples and the water resonance. The numerical results from these fits are listed in Tables 2 and 3. The dipolar relaxation rate constant $R_{DD}$ of Eq. 7 is denoted here by $R^*_{DD}$, leaving open the possibility of additional unidentified relaxation mechanisms. Clearly, water has a significant influence on the $R_{1\rho}(H)$ data. Specifically, all protons listed in Table 2 for water-free antamanide show a similar behavior, with exchange time constants $14 \le \tau_{ex} \le 27$ μs and apparent chemical shift differences between the two model sites of $119 \le \Delta_{app} \le 540$ Hz (assuming equipopulated sites with $p_A = p_B = 0.5$). In contrast, the water-containing sample shows a discernible rf field dependence only for $Val^1$ $H^N$ and $Phe^6$ $H^N$, with $\tau_{ex} = 23$ μs and $\Delta_{app} = 118$ and 111 Hz, respectively (see Table 3).

The asymptotic values $R^*_{DD}$ for high rf field strength vary significantly from site to site. For example, the $R^*_{DD}$ of $Ala^4$ $H^N$ is seven times greater than that of $Ala^4$ $H^\alpha$. The $R^*_{DD}$ values are similar for the water-free and water-containing antamanide samples, except for $Val^1$ $H^N$, where the values differ by a factor of 2.6. Particularly large $R^*_{DD}$ values are observed for $Ala^4$ $H^N$ and $Phe^5$ $H^\alpha$. For infinitely strong rf field strength, a purely dipolar $R_{DD}$ value should be obtained that depends on the distances to the nearest-neighboring protons. To obtain estimates of $R_{DD}$ values to be expected, we have used the interproton distances (assumed to be rigid, tumbling at $\tau_{rot} = 675$ ps) from the GROMOS antamanide structures (vide infra). With the exception of the water protons, the larger values of $R^*_{DD}$ (e.g. $R^*_{DD} > 5$ $s^{-1}$) cannot be accounted for by site-specific interproton distances. The possibility that some of the antamanide $R^*_{DD}$ values may contain additional contributions is further suggested by a comparison of the NOE cross-peak volumes. The ratio $R_{DD}(Ala^4\ H^\alpha, \text{water-free})/R_{DD}(Ala^4\ H^\alpha, \text{water-containing}) = 1.04$, computed from the sum of the NOE cross-peak volumes, compares well with the ratio $R^*_{DD}(Ala^4\ H^\alpha,$

TABLE 3
WATER-CONTAINING ANTAMANIDE $R_{1\rho}$ EXCHANGE PARAMETERS AT 250 K AND 600 MHz

| Proton | $\tau_{ex}$ (μs)[a] | $\Delta_{app}$ (Hz)[b] | $R^*_{DD}$ ($s^{-1}$)[c] |
|---|---|---|---|
| $Val^1$ $H^N$ | 23 | 118 | 7.59 |
| $Pro^3$ $H^\alpha$ | x | x | 3.64 |
| $Ala^4$ $H^N$ | x | x | 18.88 |
| $Ala^4$ $H^\alpha$ | x | x | 2.60 |
| $Phe^5$ $H^\alpha$ | x | x | 10.20 |
| $Phe^6$ $H^N$ | 23 | 111 | 5.75 |
| Water | 35 | 221[d] | 10.20 |

[a] x indicates that no dependence upon the rf field amplitude was observed.
[b] Assuming $p_A = p_B = 0.5$.
[c] For protons having an x, $R^*_{DD}$ is the average over the $R_{1\rho}$ values.
[d] Taking $p_A = p_{bound} = 0.82$ and $p_B = p_{free} = 0.18$.

water-free)/$R^*_{DD}$($Ala^4$ $H^\alpha$, water-containing) = 0.98, obtained from the $R_{1\rho}$(H) measurements. However, the corresponding ratio $R_{DD}$($Val^1$ $H^N$, water-free)/$R_{DD}$($Val^1$ $H^N$, water-containing) = 0.71 is larger by a factor of 1.8 than the ratio $R^*_{DD}$($Val^1$ $H^N$, water-free)/$R^*_{DD}$($Val^1$ $H^N$, water-containing). On the other hand, the large value of $R^*_{DD}$ for the water resonance can be explained well by the short intramolecular proton–proton distance.

It might be suspected that ROE cross-relaxation during the spin-lock renders some $R^*_{DD}$ values erroneously large. In the $R_{1\rho}$(H) experiments, the proton resonance of interest is excited with a frequency-selective 90° pulse of alternating phase, followed by concomitant phase alternation of the receiver. This reduces, but does not eliminate, potential ROE contributions. Accordingly, we have estimated ROE contributions using the same methods for estimating the expected $R_{DD}$ values. The results show that the ROE contributions would be insufficient to account for the large $R^*_{DD}$ values observed. We note that the excessively large $R^*_{DD}$ values for $Ala^4$ $H^N$ and $Phe^5$ $H^\alpha$ are similar in the water-free and water-containing samples. This suggests that they represent a kind of intermediate plateau in the $B_1$-field dependence. The most probable explanation for this plateau is that it reflects the presence of additional rapid motions. Such motions would have correlation times, $\tau_{unknown}$, between those affecting the $B_1$-field dependence of $R_{1\rho}$(H) and those affecting $R_1$(H) (e.g. 2 μs ≥ $\tau_{unknown}$ ≥ 2 ns). With the current range of $B_1$-field strengths, these additional motions contribute an essentially constant value to $R_{1\rho}$(H), and thus raise the $R^*_{DD}$ value above the plateau value $R_{DD}$ that would have been observed if only dipolar relaxation were operative. At this point, we refrain from speculating on the nature of these hypothetical processes.

Equation 8 suggests several possible reasons for the loss of the rf field dependence of $R_{1\rho}$(H) upon hydration. First, the water binding may directly alter the exchange time constant $\tau_{ex}$ by lowering the activation barrier, without changing the fractional populations $p_A$ and $p_B$. Alternatively, water binding could stabilize one of the two conformations, thereby changing $p_A$ and $p_B$. Third, the water could simply reduce the magnitude of the chemical shift difference $\Delta = \nu_0(\delta_A - \delta_B)$ between the two states. In this last scenario, only the sensitivity of $R_{1\rho}$(H) to dynamic effects would be affected. Although a mere chemical shift effect caused by hydration is a valid concern for $H^N$ protons whose chemical shifts are sensitive to hydrogen bonding, it is less likely for the $H^\alpha$ protons. Nonetheless, it is difficult to distinguish between the possible origins of the $R_{1\rho}$ effect for protons. In contrast, the $^{13}C^\alpha$ shifts are determined more heavily by local conformational properties, and are less sensitive to environmental effects. This was the motivation for the measurement of $^{13}C^\alpha$ relaxation rate constants discussed in the next subsection.

A comparison with the results of an earlier study of $R_{1\rho}$(H) by Blackledge et al. (1993), performed on an antamanide sample with an unspecified water content at temperatures between 275 and 320 K, shows characteristic differences. The earlier study suggested a hydrogen-bond exchange process involving the $Val^1$ and $Phe^6$ amide protons with an activation energy of ≈ 21 kJ/mol, and a lifetime of ≈ 27 μs at 320 K. Conformational searching via the MEDUSA algorithm (Brüschweiler et al., 1991) revealed $Val^1$ $H^N$---$Phe^9$ CO and $Phe^6$ $H^N$---$Ala^4$ CO as candidates for transient hydrogen bonds. It was concluded that antamanide interconverts between conformers that alternately contain and lack these hydrogen bonds, and that this interconversion process is accompanied by large changes in the torsion angles $\Psi^4$, $\Phi^5$, $\Psi^9$, and $\Phi^{10}$. $Val^1$ $H^N$ and $Phe^6$ $H^N$ are the only protons that showed a measurable rf field dependence of $R_{1\rho}$(H).

Extrapolating the results of Blackledge et al. (1993) to 250 K leads to an exchange time constant $\tau'_{ex}$ (250 K) ≈ 246 μs. This immediately shows that the process dominating the high-temperature behavior between 275 and 320 K must be different from the process relevant at 250 K, having 14 ≤ $\tau_{ex}$ ≤ 27 μs. Apparently, in addition to the dynamics process studied by Blackledge et al. (1993), there exists a faster conformational process with a lower activation energy that becomes $R_{1\rho}$-active at lower temperature. The observation that the $\tau'_{ex}$ process does not cause excessive line broadening of the $Val^1$ $H^N$ and $Phe^6$ $H^N$ resonances at 250 K must be due to a fortuitous near-degeneracy of the temperature-dependent chemical shifts of the involved conformers, or to a disproportionate preference for a particular conformer.

Nevertheless, it is striking that the observations of Blackledge et al. (1993) closely match the results of the water-containing antamanide at 250 K, where also only $Val^1$ $H^N$ and $Phe^6$ $H^N$ show a measurable rf field dependence of $R_{1\rho}$(H). Indeed, the chemical shifts seem to indicate that the sample used by Blackledge et al. (1993) contained traces of water, although considerably less than the presently studied sample.

A comparison of the values listed in Tables 2 and 3 suggests that water binding enhances the rigidity of the peptide ring, most likely by cross-linking opposite sides of the ring. This stabilizing role of water is also suggested by the MD simulations described later.

$R_{1\rho}(H)$ measurements as a function of rf field strength were also performed for the water resonance, and the resulting fit versus rf field strength by Eq. 6 is given in Fig. 3d. The data suggest that water also experiences an exchange process, which modulates its chemical shift. A fit by Eqs. 6–8 gives $\tau_2 = 35$ μs, $p_A p_B \Delta^2 = 7225$ Hz$^2$, and $R_{DD} = 10.2$ s$^{-1}$. An interpretation of $\tau_2$ and $p_A p_B \Delta^2$ will be given in the Discussion section.

*Comparison of $^{13}C^{\alpha}$ relaxation rate constants*

Measurements of $^{13}C^{\alpha}$ relaxation included the longitudinal relaxation rate constant, $R_1$, the transverse relaxation rate constant, $R_2$, and the heteronuclear NOE. Values for the rate constants are provided in Tables S3a,b,c (Supplementary Material). For the water-free sample, the average $R_1$ is 3.46 s$^{-1}$ ± 0.15 s$^{-1}$, and the average NOE is 0.49 ± 0.03. For the water-containing sample, the average $R_1$ is 3.56 s$^{-1}$ ± 0.08 s$^{-1}$, and the average NOE is 0.45 ± 0.03. The quoted errors are the mean individual rms error estimates. Thus, there is no significant difference between the $R_1$ and NOE values in the presence and absence of water.

In contrast, the $^{13}C^{\alpha}$ $R_2$ measurements show large variations along the peptide backbone, as well as large differences between the two antamanide samples. This is visualized in Fig. 4. The largest values of $R_2$ are found for Ala$^4$ $C^{\alpha}$, Phe$^5$ $C^{\alpha}$, and Phe$^6$ $C^{\alpha}$ in both samples, followed by Phe$^9$ $C^{\alpha}$, and Phe$^{10}$ $C^{\alpha}$. Figure 4 demonstrates that the interaction with water strongly reduces the $R_2$ values of Ala$^4$, Phe$^5$, and Phe$^6$. In contrast, the water does not significantly alter the other $C^{\alpha}$ $R_2$ values. The large $R_2$ values reflect the presence of slow conformational exchange dynamics.

Similar manifestations of conformational exchange in antamanide have been observed in an earlier $^{13}C$ relaxation study (Bremi et al., 1994) on a water-free antamanide sample at 320 K. The earlier study showed significant exchange contributions in $^{13}C^{\alpha}$ $R_2$ for Ala$^4$ and Phe$^5$, as well as for Phe$^9$ and Phe$^{10}$. Unlike what is found in the

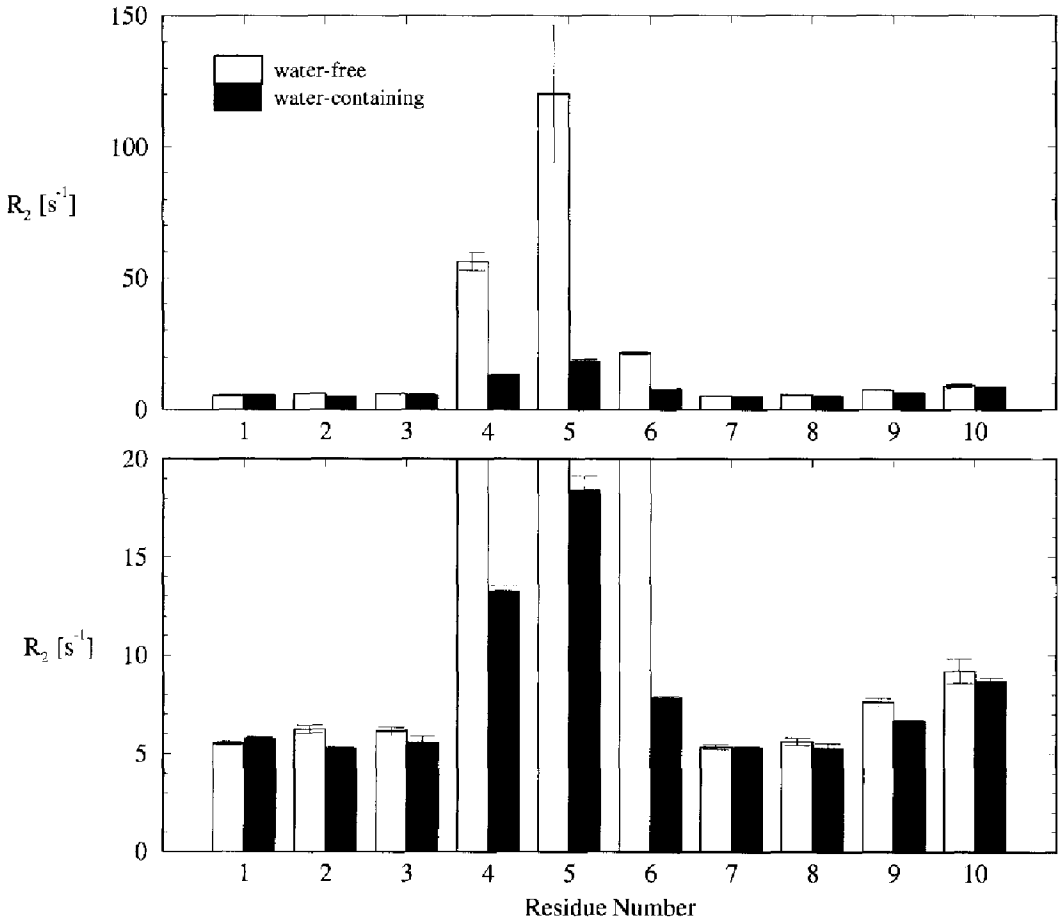


Fig. 4. $^{13}C^{\alpha}$ transverse relaxation rate constants $R_2 = 1/T_2$ for the 10 residues in antamanide measured at natural $^{13}C$ abundance. The light and dark bars refer to water-free and water-containing antamanide, respectively. The upper panel gives the full range of $R_2$ values, while the lower panel shows a vertical expansion by a factor of 7.5. The experimental variance of the data is indicated.

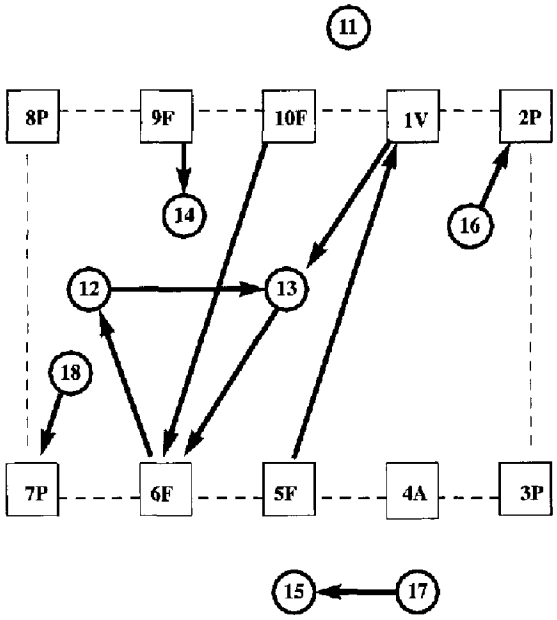


Fig. 5. Hydrogen bonding of the eight water molecules in the crystal structure of antamanide, which served as the starting conformation of the MD simulations. The circled numbers represent the water molecules (numbered from 11 to 18), and the boxes represent the amino acid residues. The arrows indicate the donor → acceptor direction.

present study, the magnitude of those exchange contributions was approximately 'symmetric' across the peptide ring; thus, the increases at Ala[4] and Phe[5] were similar to those at Phe[9] and Phe[10]. Therefore, the temperature dependence of the backbone conformational exchange process appears to vary across the peptide ring.

The spectral density function of the model by Lipari and Szabo (Eq. 13; Lipari and Szabo, 1982a,b) permits a description of the dipolar contribution to the $^{13}C^{\alpha}$ antamanide relaxation data in terms of motional parameters $\tau_{ik}$ and $S_k^2$ of the $C_k^{\alpha}$-$H_k^{\alpha}$ bonds. The much smaller CSA contribution to relaxation of the $^{13}C^{\alpha}$ nucleus is most likely negligible (Naito et al., 1981,1983; Janes et al., 1983; Naito and McDowell, 1983). The $C^{\alpha}$ $R_2$ data clearly indicate the presence of additional slower conformational exchange dynamics, represented in Eq. 10 by the $R_{ex}^{(k)}$ term. $R_{ex}^{(k)}$ may vary from carbon site to carbon site. Thus, for n residues, 3n + 1 fitting parameters must be adjusted. As we have measured only three relaxation parameters per residue, such a fit is not warranted. However, the near uniformity of the $C^{\alpha}$ $R_1$ and NOE values along the antamanide backbone for both samples also suggests uniformity of the rapid intramolecular local dynamics. This leads to the use of a single short correlation time $\tau_j$, which we have fixed at 20 ps. Thus, only $S_k^2$ and $R_{ex}^{(k)}$ need to be determined for each $C_k^{\alpha}$-$H_k^{\alpha}$ bond, in addition to the overall rotational correlation time, $\tau_{rot}$.

Studies of protein backbone dynamics by heteronuclear relaxation rate measurements often use the ratio of $R_2/R_1$ to obtain a first estimate of $\tau_{rot}$ (Kay et al., 1989; Palmer et al., 1991). In the absence of exchange effects, and if the internal motion of the $C_k^{\alpha}$-$H_k^{\alpha}$ vectors is in the extreme narrowing regime, this ratio depends only on $\tau_{rot}$. Unfortunately, this approach is not advisable for antamanide, since the $R_2$ values are clearly biased by an exchange contribution $R_{ex}$. Nor is it advisable to extract $\tau_{rot}$ from $R_1$ values alone, assuming $S^2 = 1$, which would lead to erroneously small values of $\tau_{rot}$. Instead, we have exploited the fact that the steady-state heteronuclear NOE ($R_c\gamma_H/R_1\gamma_C$) depends only on $\tau_{rot}$ if $\tau_i \ll \tau_{rot}$, and have therefore used the heteronuclear NOEs to estimate an initial value for $\tau_{rot}$.

A procedure based on that of Dellwo and Wand (1989) was then used in a second step to find optimal values of $S_k^2$ and $\tau_{rot}$ from the $R_1$ and NOE data. Specifically, $S_k^2$ was varied for each $C^{\alpha}$-$H^{\alpha}$ bond with $\tau_{rot}$ held fixed, in order to minimize the $\chi_k^2$ error function given by:

$$\chi_k^2 = \left(\frac{R_1^{(k)} - R_{1mf}^{(k)}}{\sigma_{R_1}^{(k)}}\right)^2 + \left(\frac{R_c^{(k)} - R_{cmf}^{(k)}}{\sigma_{R_c}^{(k)}}\right)^2 \qquad (14)$$

$R_{1mf}^{(k)}$ and $R_{cmf}^{(k)}$ denote the $C^{\alpha}$ longitudinal and heteronuclear cross-relaxation rate constants derived from the model function $J_{CH}(\omega)$, given in Eq. 13. The sigma factors in the denominator are the aforementioned estimated errors in the experimental rate constants. After minimization of $\chi_k^2$, $\tau_{rot}$ was stepped and new $S_k^2$ values were determined. In this fashion, a grid search for $\tau_{rot}$ was performed until a local minimum was found for the sum $\chi^2 = \Sigma_k \chi_k^2$ (Dellwo and Wand, 1989). The final values of $\tau_{rot}$ and $S_k^2$ were used together with $\tau_i$ to compute the dipolar contribution to $R_2$ in Eq. 10. The differences between these computed $R_2$ values and the experimental ones are the exchange contributions $R_{ex}$.

Table S4 in the Supplementary Material lists the fitted $S_k^2$ and $R_{ex}^{(k)}$ values versus peptide sequence for both antamanide samples. The resulting overall rotational correlation time, $\tau_{rot}$, for the water-free sample is 660 ± 10 ps/rad, and it is 690 ± 10 ps/rad for the water-containing sample. The small difference in $\tau_{rot}$ reflects the difference in the average heteronuclear NOEs, which is believed to be insignificant. The $S_k^2$ values do not change significantly between water-free and water-containing antamanide. In both cases, $S_k^2$ falls in the range $0.78 < S^2 < 0.89$ and shows little variation among the residues. Such uniformity is to be expected, considering the rather uniform $R_1$ and NOE data. The $S_k^2$ values are comparable to those obtained in previous heteronuclear relaxation studies of $C^{\alpha}$ carbons (Dellwo and Wand, 1989; Palmer et al., 1991), and reflect fast local $C^{\alpha}$-$H^{\alpha}$ bond librations, usually occurring on time scales in the lower picoseconds. Thus, the water molecules have apparently little or no effect on these fast internal dynamics.

In contrast, the presence of water greatly reduces the $R_{ex}$ contributions to $R_2$. As with the proton $R_{1\rho}(H)$ meas-

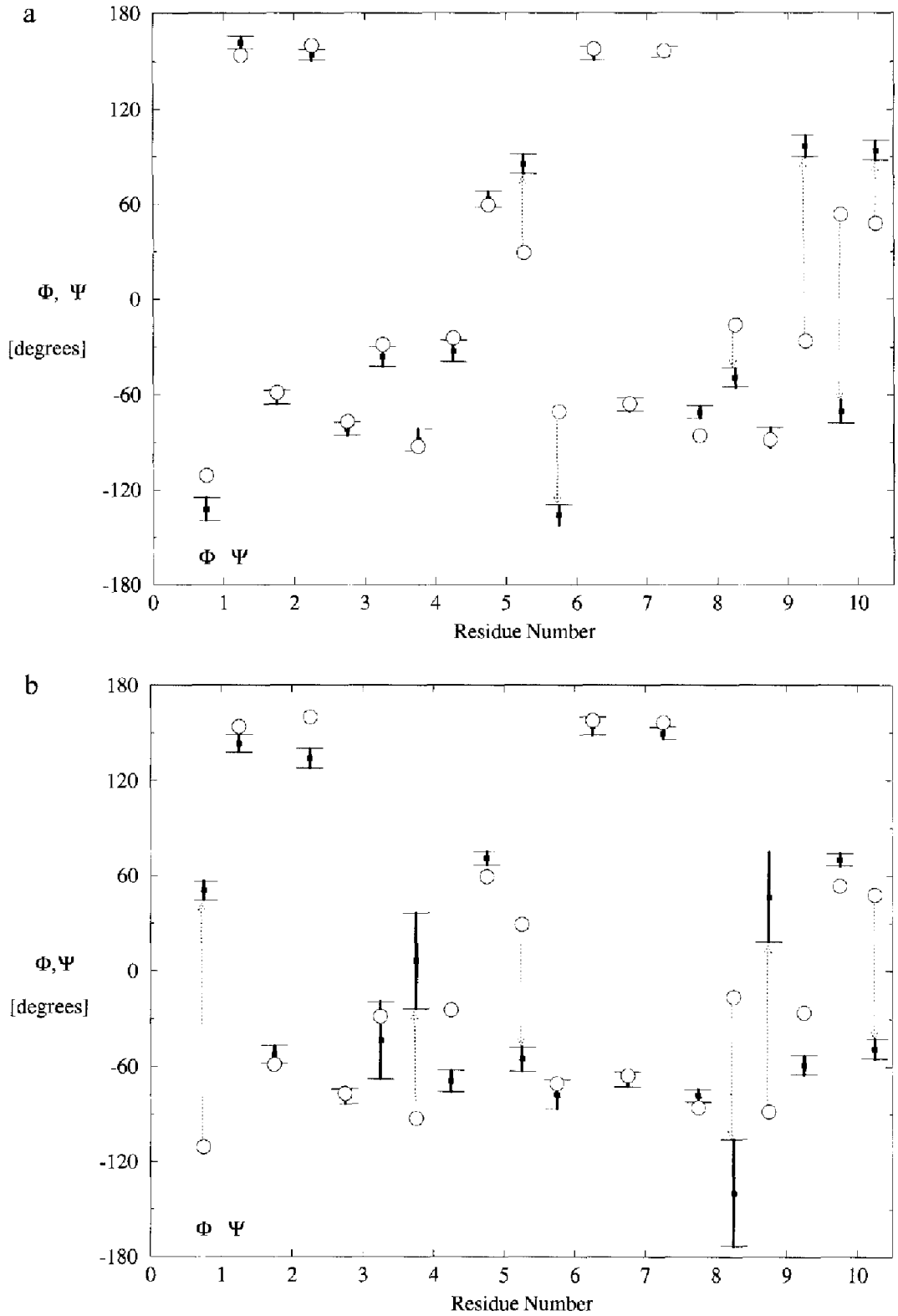


Fig. 6. The Φ and Ψ dihedral angles as functions of the residue number, averaged over 600 ps of MD trajectory (time 400–1000 ps). The bars represent the rms fluctuation of the dihedrals over this time period. The open circles denote the dihedral angle values of the crystal structure starting conformation. (a) The simulation with eight water molecules; and (b) the simulation without water.

urements, the reduction of $R_{ex}$ upon the addition of water could signify a direct perturbation of the exchange process, or merely a loss of sensitivity to the exchange dynamics due to a water-induced reduction of the $C^{\alpha}$ chemical shift difference. While the latter possibility is a valid concern for $H^{N}$ protons, it is less likely for the $C^{\alpha}$ nuclei

due to the fact that the principal determinants of the $C^{\alpha}$ shifts are the local backbone $\Phi$, $\Psi$, and $\chi$ torsion angles (Spera and Bax, 1991; Wishart et al., 1991; de Dios et al., 1993a,b). Accordingly, the reduction in the $C^{\alpha}$ $R_2$ values most likely reflects indeed a genuine perturbation of the exchange process by water on the microsecond time scale.

The sensitivity of the $C^{\alpha}$ chemical shifts to changes in $\Phi$ and $\Psi$ suggests that the chemical exchange involves transitions of the torsion angles of $Ala^4$, $Phe^5$, $Phe^6$, $Phe^9$, and $Phe^{10}$. These two contiguous segments correspond to the regions of enhanced torsion angle flexibility identified by the earlier studies of Blackledge et al. (1993), involving $\Psi^4$, $\Phi^5$, $\Psi^5$ and $\Psi^9$, $\Phi^{10}$, $\Psi^{10}$, $\Phi^1$, $\Psi^1$. The reduction of the $R_{ex}$ contribution to $R_2$ in the presence of water suggests that the dynamics of these regions is affected by the binding of water molecules.

To estimate a time scale for the backbone exchange dynamics, one can use the fact that the $R_2$ CPMG spin-echo sequence suppresses slow exchange effects with rate constants $k_{ex} \ll \delta_{CPMG}^{-1}$ (Bloom et al., 1965). $\delta_{CPMG}$ denotes the half period of the spin-echo unit $(\delta_{CPMG}\text{-}180°\text{-}\delta_{CPMG})_n$. For the measurements performed here, $\delta_{CPMG} = 500$ μs and the 180° refocusing pulses were 75 μs, resulting in a pulse duty cycle of 7%. The fact that the $R_2(^{13}C^{\alpha})$ values are much larger for $Ala^4$, $Phe^5$, and $Phe^6$ than for the other residues in both antamanide samples indicates that exchange processes exist with $k_{ex} > 2 * 10^3\ s^{-1}$. In an attempt to determine the exchange time constant more precisely, we also performed $R_{1\rho}$ ($^{13}C^{\alpha}$) measurements on the water-free antamanide sample with rf field strengths of 6.67 and 1.69 kHz for the CW spin-lock. We have not found a significant rf field dependence. Moreover, the $R_{1\rho}(^{13}C^{\alpha})$ values were the same as those obtained with the CPMG sequence. Unfortunately, the use of stronger rf field strengths was not feasible. Thus, the current $R_{1\rho}(^{13}C^{\alpha})$ data suggest that the time constants for the conformational exchange processes in the water-free sample are less than $(2\pi * 6.77\ \text{kHz})^{-1} \approx 24$ μs. This upper limit should be compared with the values of $\tau_{ex}$ in Table 2, determined by the proton $R_{1\rho}(H)$ measurements. Although there is no major contradiction, the measurements should have shown a noticeable rf field amplitude dependence. It may

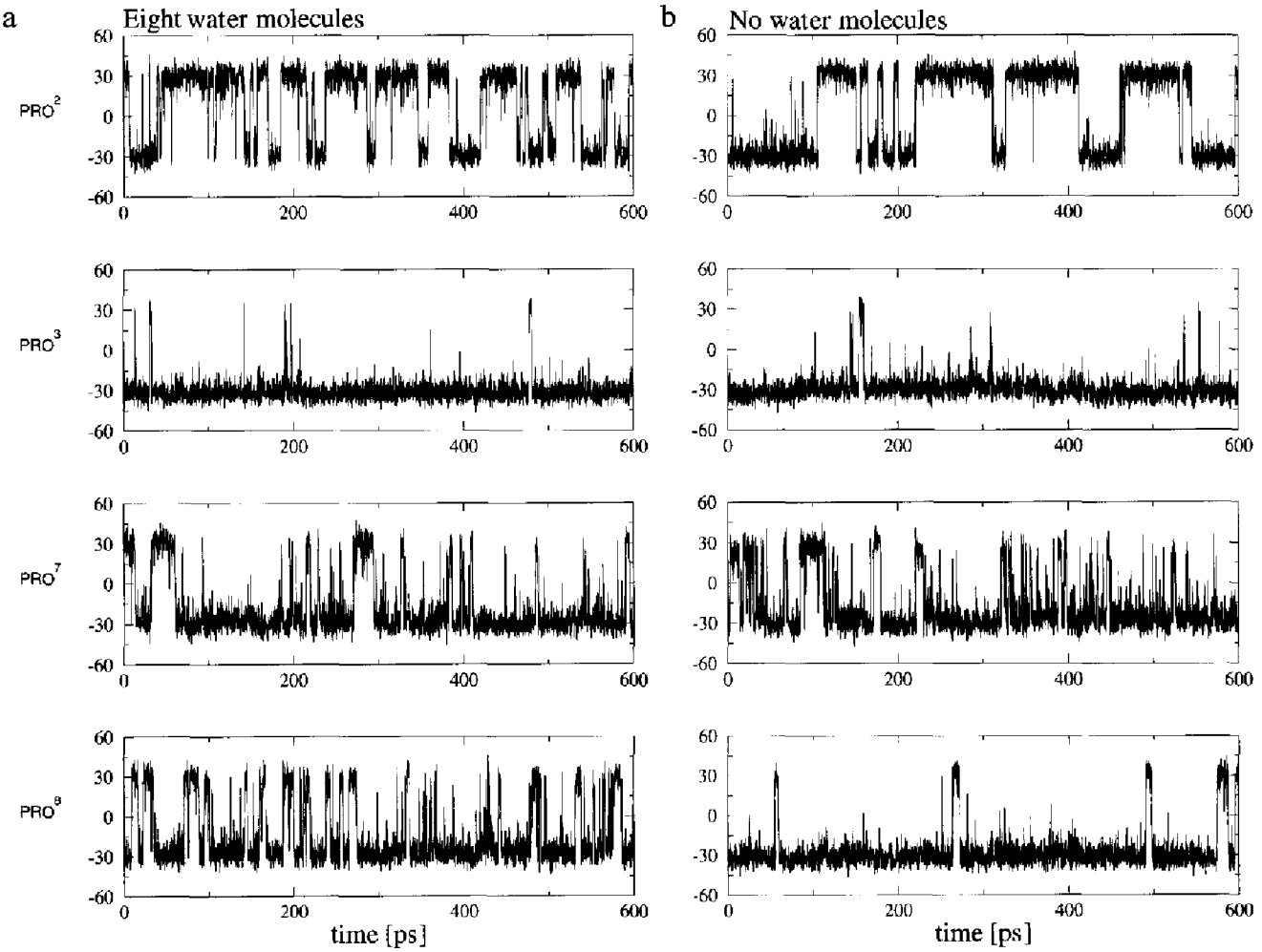


Fig. 7. $\chi^2$ angle trajectories of the four prolines in antamanide, indicating the proline puckering over the 600 ps analysis period. (a) The simulation with eight water molecules; and (b) the simulation without water.

TABLE 4
ANTAMANIDE PROLINE PUCKERING RESIDENCY TIMES[a]

| Residue | Eight water molecules | | No water molecules | |
|---|---|---|---|---|
| | $\langle\tau\rangle$ (ps) | $\tau_{max}$ (ps) | $\langle\tau\rangle$ (ps) | $\tau_{max}$ (ps) |
| $Pro^2$ | 16 | 71 | 18 | 110 |
| $Pro^3$ | 45 | 165 | 44 | 226 |
| $Pro^7$ | 15 | 95 | 7 | 52 |
| $Pro^8$ | 9 | 57 | 59 | 196 |

[a] Averaged residence times are denoted by $\langle\tau\rangle$, maximal values by $\tau_{max}$.

be that this has gone unnoticed due to the poor sensitivity of the natural-abundance $^{13}C$ experiments.

*Molecular dynamics simulations*

The NMR results described above are complemented by a series of six MD simulations, which provide an atomic description of the antamanide–water system. The initial conformation was taken from the crystal structure (Karle et al., 1979). In this structure, antamanide is associated with eight water molecules. It exists in a 'basket'-like form with five water molecules held within the 'basket' in hydrogen-bonding distance of the peptide, as shown schematically in Fig. 5. Water molecule 13 is involved in a cross-ring bridging network of hydrogen bonds between $Val^1$ and $Phe^6$. The peptide also forms two cross-ring hydrogen bonds between $Phe^{10}$ $H^N$ and $Phe^6$ CO and between $Phe^5$ $H^N$ and $Val^1$ CO.

*Simulation (i) with eight water molecules*

In the 1 ns simulation of antamanide with all eight water molecules present, the peptide remained fairly rigid. The positional rms difference between the starting crystal structure and the final conformation is 0.80 Å for the $C^\alpha$ atoms, and 1.67 Å for all non-hydrogen atoms. In Fig. 6a, the average values of the $\Phi$ and $\Psi$ dihedral angles are plotted with their rms fluctuations over the 600 ps analysis period, and are compared with the dihedral angles of the crystal structure. They show only slight fluctuations around their mean position during the analysis period, and remain close to the values of the crystal structure, except for $\Psi^5$, $\Phi^6$, $\Psi^8$, $\Psi^9$, $\Phi^{10}$, and $\Psi^{10}$. Figure 7a shows the $\chi^2$ angles of the four prolines as functions of the simulation time. All four dihedral angles show bistable fluctuations, where the frequency of transition varies from proline to proline. Table 4 gives the average and maximum residence times in the two conformations for the four prolines.

The hydrogen-bonding network present during the analysis period is shown in Fig. 8a, indicating the fractional time of existence for each bond. All eight water molecules remain closely associated with the peptide. Only one of the two intramolecular hydrogen bonds survives. On the other hand, the hydrogen-bonding interactions with the water molecules are more extensive than in the initial crystal structure conformation. The molecule can still be described as a basket which contains six of the eight water molecules. Water molecule 13 is located at the bottom of the basket and forms strong hydrogen bonds to $Val^1$, $Phe^6$, and $Phe^9$ and also to four other water molecules. This water molecule, through its extensive hydrogen bonding, appears to stabilize the conformation of the peptide and of the water-binding network. The other water molecules (except for no. 14) also contact the peptide, but to varying and lesser degrees. Water molecules 11 and 14 sit on top of the basket and form hydrogen bonds with the other water molecules. The water molecules 15 and 17 remain on the outside of the peptide ring and maintain hydrogen bonds between each other and to $Ala^4$ and $Phe^5$. Figure 9 shows the final structure reached at the end of the simulation period in stereographic form.

*Simulation (ii) without water molecules*

In a 1 ns simulation of water-free antamanide in chloroform, the peptide changed its configuration significantly from its starting conformation. The positional rms difference between the initial crystal structure and the final structure is 1.7 Å for $C^\alpha$ atoms, and 2.7 Å for all non-hydrogen atoms. The conformational change occurs over the first few hundred picoseconds. The molecule leaves its basket conformation, seen in the previous simulation with water, and collapses into a more compact structure. Figure 6 shows that some of the dihedral angles differ by large amounts between the water-free and eight-water conformations. Removal of the eight water molecules seen in the crystal structure resulted in the following changes

TABLE 5
RMS FLUCTUATIONS OF THE PEPTIDE ATOMS IN THE SIMULATIONS

| Number of water molecules | Analysis period (ps) | Temperature (K) | Rms fluctuations of $C^\alpha$ atoms (Å) | Rms fluctuations of non-hydrogen peptide atoms (Å) |
|---|---|---|---|---|
| 0 | 600 | 250 | 0.50 | 0.93 |
| 1 | 300 | 250 | 0.30 | 0.75 |
| 1 | 300 | 250 | 0.26 | 0.56 |
| 2 | 300 | 250 | 0.37 | 1.12 |
| 8 | 600 | 250 | 0.31 | 0.65 |
| 8 | 300 | 290 | 0.27 | 0.58 |

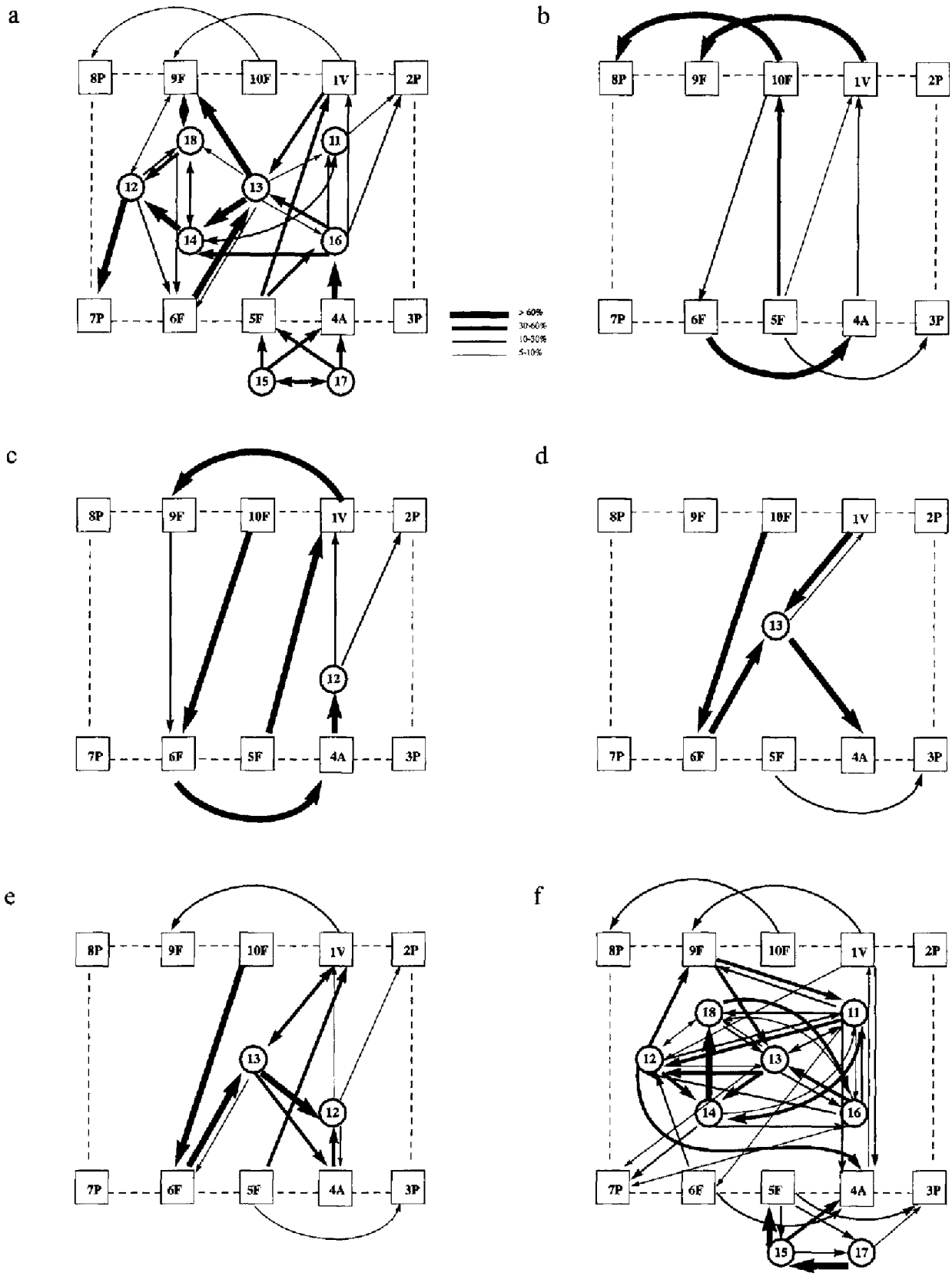


Fig. 8. Hydrogen-bonding patterns in the water–antamanide complex in the course of the analysis period. The arrows indicate the donor→acceptor direction. The widths of the arrows indicate the percentage of time during which a particular hydrogen bond was present. (a) The simulation with eight water molecules over 600 ps; (b) the simulation without water molecules over 600 ps; (c) the simulation with water molecule 12 over 300 ps; (d) the simulation with water molecule 13 over 300 ps; (e) the simulation with two water molecules, 12 and 13, over 300 ps; and (f) the simulation with eight water molecules over 300 ps at 290 K.

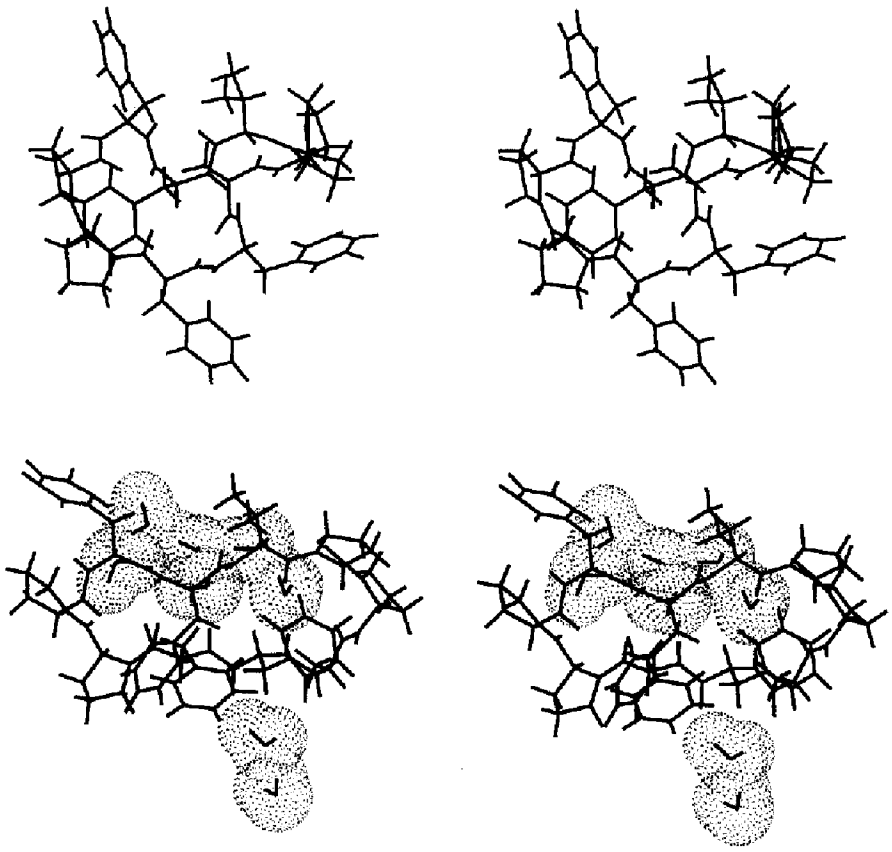

Fig. 9. Stereographic representation of antamanide with no water (top) and with eight water molecules (bottom). The structures are taken from 600 ps molecular dynamics simulation trajectories described in the text.

in the backbone dihedral angles: $\Delta\Phi^1$: 180°, $\Delta\Phi^4$: 90°, $\Delta\Psi^5$: 140°, $\Delta\Phi^6$: 60°, $\Delta\Psi^8$: −90°, $\Delta\Phi^9$: 130°, $\Delta\Psi^9$: −160°, $\Delta\Phi^{10}$: 140°, and $\Delta\Psi^{10}$: −140°.

The rms fluctuations around the average Φ-Ψ dihedral values (Fig. 6b) are similar to what is seen when water is present, with the exception of the dihedrals $\Psi^3$ and $\Phi^4$, which determine the orientation of the peptide plane between residues 3 and 4, and the dihedrals $\Psi^8$ and $\Phi^9$, which determine the orientation of the peptide plane between residues 8 and 9. Figure 10 shows the fluctuations of these two peptide planes as a function of time. The peptide plane between residues 3 and 4 actually flips twice during the analysis period, whereas the peptide plane between residues 8 and 9 flips only once. While these peptide flips are not statistically significant, the fact that three such transitions were observed during the 600 ps analysis period and none in the simulation with eight water molecules indicates that the peptide may be more flexible in the absence of water.

The proline puckering without water, visualized in Fig. 7b, shows that $Pro^3$ and $Pro^8$ appear to prefer the conformation with $\chi^2 = -30°$. In contrast, $Pro^2$ and $Pro^7$ fluctuate more evenly between the conformations with $\chi^2 = \pm 30°$. This difference in the proline puckering has been reported previously (Brunne et al., 1993; Schmidt et al., 1993). The average time interval between transitions, $\langle\tau\rangle$ (Table 4), is in better agreement with the experimental data (Mádi et al., 1990) than the previous GROMOS simulation using a stochastic treatment of solvent effects (Brunne et al., 1993). This is an indication that the all-atom model of chloroform used here yields more accurate results than the previously used mean force field and stochastic dynamics for the chloroform solvent. Figures 7a and b also indicate that particularly the puckering motion of $Pro^8$ is influenced by the presence of water, which seems to slightly shift the equilibrium towards the conformation with $\chi^2 = -30°$.

The hydrogen-bonding pattern of antamanide in the absence of water contains three hydrogen bonds that are established for more than 68% of the time (Fig. 8b). The hydrogen-bonding patterns for antamanide without water, previously studied by Blackledge et al. (1993), and the present patterns have features in common, most notably the hydrogen bonds between $Val^1$ and $Phe^9$, and between $Phe^6$ and $Ala^4$. Also the hydrogen bonds $Ala^4$-$Val^1$, $Phe^5$-$Val^1$, and $Phe^{10}$-$Phe^6$ are present in the preferred conformational pair of Blackledge et al. (1993). The hydrogen bond $Phe^{10}$-$Phe^8$ occurs in some less favored conformations of the previous study, while the hydrogen bonds $Phe^5$-$Pro^3$ and $Phe^5$-$Phe^{10}$ do not appear among the eight conformational pairs of lowest energy. Differences are not unexpected, taking into account the

limited coverage of the conformational space by the MD simulations, and the fact that the sample investigated by Blackledge et al. (1993) was probably not completely water-free.

*Simulations (iii) and (iv) with one water molecule*

To gain further insight on how water molecules interact with antamanide, two simulations with water molecules 12 and 13 were performed where only a single water molecule was associated with antamanide in the chloroform bath. Water molecule 13 remained at the 'bottom of the basket' in the fully hydrated peptide during the hydrated simulation. Water molecule 12 was located more at the top layer of the basket in the starting X-ray conformation. In these two 400 ps simulations, the peptide settled into two distinct conformations that probably represent two low-energy conformations of the system. The simulation with water molecule 12 has an rms positional difference for the $C^{\alpha}$ atoms between the starting conformation and the final conformation of 1.2 Å, whereas the simulation with water molecule 13 has an rms positional difference of 0.5 Å for the same atoms.

The hydrogen-bonding patterns of these two simulations show differences. In the simulation with water molecule 12 (Fig. 8c), the water molecule is accepting a long-lived hydrogen bond from $Ala^4$ and donating two infrequent ones to the carbonyls of $Val^1$ and $Pro^2$. All long-lived intramolecular hydrogen bonds are also seen in the simulation without water, but some are populated less of the time (Fig. 8b).

In the simulation with water molecule 13 (Fig. 8d), only the intramolecular hydrogen bond between residues $Phe^{10}$ and $Phe^6$ is maintained for a high percentage of the time. The water molecule remains at the 'bottom of the basket' and is strongly hydrogen bonded, accepting bonds from $Val^1$ and $Phe^6$ while donating to $Ala^4$. On the time scale of these simulations, the two conformations with water molecules 12 or 13 do not interconvert and the strength of the hydrogen bonds suggests fairly rigid structures.

*Simulation (v) with two water molecules*

After a 400 ps simulation using simultaneously water molecules 12 and 13, the system equilibrates into yet another conformation, which seems to be intermediate between the two conformations sampled in the two sin-

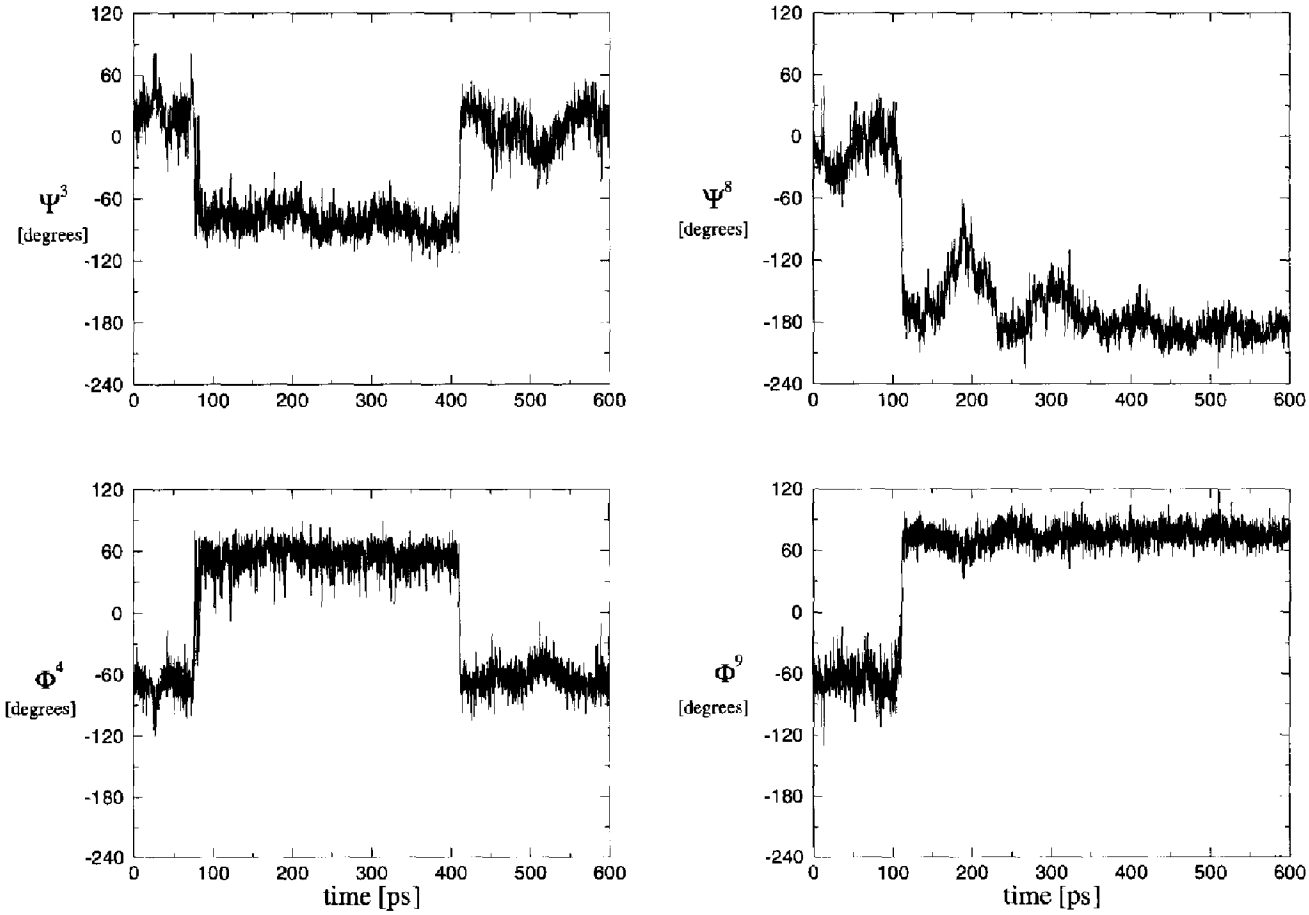


Fig. 10. Dihedral angles $\Psi^3$, $\Phi^4$, $\Psi^8$, and $\Phi^9$ involved in peptide bond flips during the 600 ps simulation of antamanide without water.

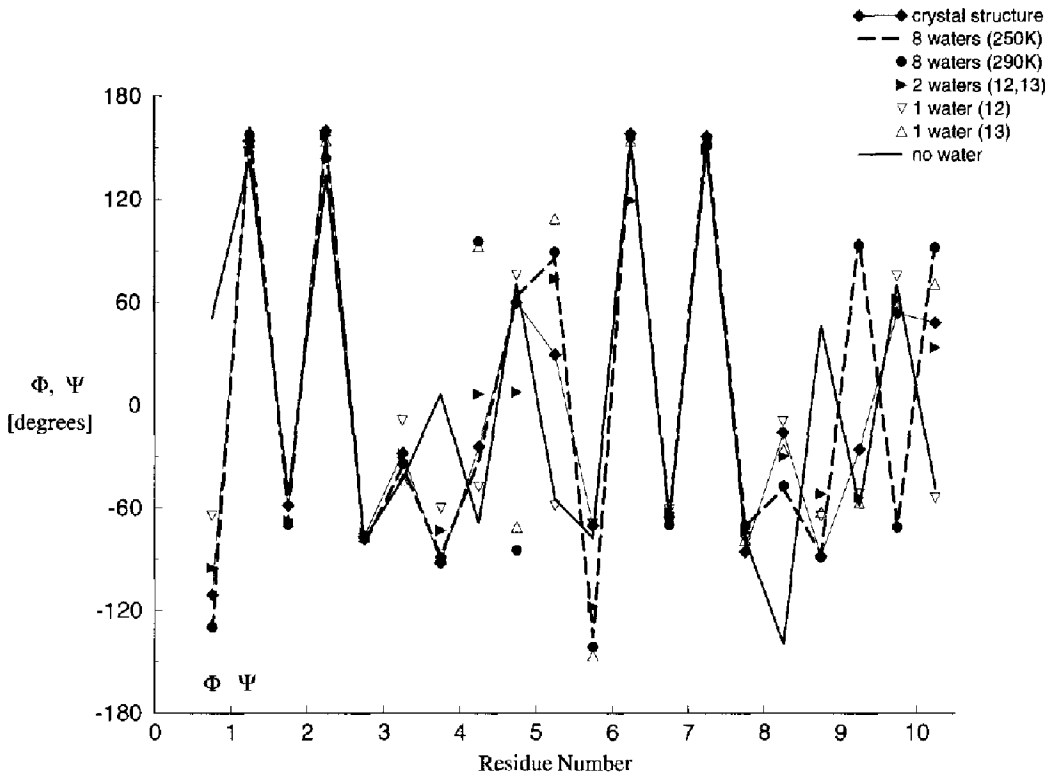


Fig. 11. Φ and Ψ dihedral angles averaged over the analysis periods for the six simulations described in the text and for the values computed from the crystal structure.

gle-water simulations. The positional rms difference between the final structure and the initial crystal structure is 0.7 Å for the $C^{\alpha}$ atoms, which is between the two values obtained from the simulations with a single water molecule.

The hydrogen-bonding pattern from this simulation also reflects the fact that it is an intermediate configuration (Fig. 8e). All but one (between $Phe^6$ and $Ala^4$) of the major hydrogen bonds seen in the simulation with water molecule 12 (Fig. 8c) are present, as are all the major hydrogen bonds in the simulation with water molecule 13 (Fig. 8d). Among some additional hydrogen bonds, water molecule 13 donates a hydrogen bond to water molecule 12. The hydrogen bonds are for the most part shorter-lived than those seen in the single-water simulations, implying that the system may be in an equilibrium between several low-energy configurations.

*Simulation (vi) with eight water molecules at elevated temperature*

The previous simulation with eight water molecules was continued for an additional 400 ps at an elevated temperature of 290 K, to investigate the stability of the positions of the water molecules. Antamanide maintained its basket conformation during the entire simulation, and the water molecules remained closely associated with it. The positional rms difference between the initial and the final structure is 0.7 Å for the $C^{\alpha}$ atoms, i.e., lower than the 0.8 Å found with the lower temperature simulation.

The hydrogen-bonding pattern to the water molecules has changed considerably (Fig. 8f). Most significantly, water molecule 13 is no longer at the 'bottom of the basket', its previously dominant hydrogen bonds from $Val^1$ and $Phe^6$ are broken, and no other water molecule has moved in to take its position. The six water molecules in the basket are more extensively hydrogen-bonded to each other than they are to the peptide. To replace the water interactions, the peptide establishes more intramolecular hydrogen bonds. Thus, although the backbone of the peptide remains near to the crystal conformation, the associated water molecules have rearranged themselves.

*Comparison between the simulations*

Water seems to stabilize several low-energy conformations. On the time scale of the MD simulation, these conformations do not interconvert. In Fig. 11 the average Φ-Ψ dihedral values from the various simulations are plotted. As mentioned before, the spread for some of the angles is very large, in particular for $\Phi^1$, $\Psi^4$, $\Phi^5$, $\Psi^5$, $\Psi^8$, $\Phi^9$, $\Psi^9$, $\Phi^{10}$, and $\Psi^{10}$. For most angles, the zero-water and eight-water structures are at opposite ends of the distributions, with the exception of $\Psi^4$ and $\Phi^5$, where the eight-water simulation reaches extreme values only after a temperature increase to 290 K.

Table 5 shows the rms positional fluctuations. The largest fluctuations for the backbone atoms are seen in

the simulation without water molecules. Water seems to play a stabilizing role. Water is involved with an extensive network of hydrogen bonds that need to be disrupted in order for a conformational transition to occur. The second most flexible configuration is the one with two water molecules present. The rms fluctuation in this simulation for all non-hydrogen atoms is 1.1 Å, the largest for the set of simulations. This is probably due to the interconversion between several low-energy conformations, which is also indicated by hydrogen bonds with an occurrence of less than 50% (Fig. 8e). The simulation with water molecule 13 alone yields the most stable configuration. This water position seems to be particularly important for stabilizing the peptide conformation.

## Discussion

*Water dynamics and NOESY data*

As stated in the NMR Results section, the vanishing of the intermolecular water–antamanide NOEs at 271 K suggests an intra-complex mobility of the associated water–antamanide interproton vectors. The mobility can be analyzed using the Lipari–Szabo parameters $\tau_{rot}$, $S^2_{water-ant}$ and $\tau_{i,water-ant}$, based on Eq. 13. A value of $\tau_{rot}(271\ K) \approx 460$ ps can be estimated from $\tau_{rot}(250\ K) = 675$ ps by accounting for the direct and viscosity-mediated temperature effects in the Stokes–Einstein relation. A numerical treatment of Eqs. 4 and 13, using $\tau_{rot}(271\ K) = 460$ ps, then shows that NOE cross peaks will vanish if $S^2_{water-ant}(271\ K) < 0.5$, with $\tau_{i,water-ant}(271\ K)$ either in the range $5\ ps < \tau_{i,water-ant}(271\ K) < 80$ ps, or in a longer timescale range $220\ ps < \tau_{i,water-ant}(271\ K) < 800$ ps. Note that $S^2_{water-ant}(271\ K)$ values near 0 are unlikely, since this would lead to the quenching of the NOEs at higher temperature; such quenching is not consistent with the reappearance of the water–antamanide NOEs at 293 K. To help distinguish between the two possible $\tau_{i,water-ant}(271\ K)$ ranges, we consider the dipolar component $R_{DD}$ of the water proton $R_{1\rho}(H)$ at 250 K (cf. Eq. 6). $R_{DD}$ may be expressed as the sum $R_{DD} = R_{DD,water-water} + R_{DD,water-ant}$, where $R_{DD,water-water}$ denotes the contribution of the intramolecular dipolar interaction between the two water protons, and $R_{DD,water-ant}$ denotes the intermolecular dipolar interactions that also give rise to the water–antamanide NOEs. $R_{DD,water-water}$ can be estimated by using Eq. 13 with $\tau_{rot}(250\ K) = 675$ ps in the like-spin expression for $R_{DD}$ (Abragam, 1961). We require that $R_{DD,water-water}$ be less than the observed $R_{DD}$ value of 10.2 $s^{-1}$. This constraint can be satisfied only if the vector connecting the two water protons experiences a dynamic process at 250 K, having $S^2_{water-water} \leq 0.5$, and $\tau_{i,water-water} \approx 100$ ps. If we assume that $\tau_{i,water-ant}$ is in the same range as $\tau_{i,water-water}$, and that $\tau_{i,water-ant}$ and $S^2_{water-ant}$ remain the same or increase with decreasing temperature, then we can rule out the range $220\ ps < \tau_{i,water-ant}(271\ K) < 800$ ps. In short, the use of a Lipari–Szabo spectral density function (Eq. 13) to explain the behavior of the water–antamanide NOEs and the water $R_{DD}$ data indicates a fast dynamic process for the water molecules with a characteristic time constant $\tau_1 \approx 100$ ps.

*Identification of water dynamic processes*

Two yet unidentified processes with correlation times $\tau_1 \approx 100$ ps and $\tau_2 \approx 35$ μs are associated with the water exchange dynamics. The $\tau_1$ process is needed to explain the behavior of the water–antamanide NOESY cross peaks, and the $\tau_2$ process appears to modulate the water chemical shifts and leads to the dispersion of $R_{1\rho}(H_2O)$ with rf field strength. The MD simulations suggest that water remains bound to antamanide within at least 600 ps, and that exchange between different binding sites is infrequent.

The following physical processes have to be considered in the context of water exchange for hydrated antamanide in chloroform solution:

(i) Molecular tumbling of the water–antamanide complex with a correlation time $650\ ps < \tau_{rot} < 700$ ps at 250 K.

(ii) Conformational dynamics of antamanide with a correlation time $14\ \mu s \leq \tau_{ex} \leq 27\ \mu s$ at 250 K.

(iii) Bending and torsional dynamics of bound water with a correlation time $\tau_{local}$.

(iv) Water exchange dynamics between different binding sites with a correlation time $\tau_{site}$.

(v) Exchange dynamics between free and bound water with a correlation time $\tau_{hydrate}$.

It should be noted that during the processes (i)–(iv) a water molecule remains associated with a particular antamanide molecule, while during process (v) the association is broken and upon the next encounter a hydrogen bond to an arbitrary antamanide molecule in an arbitrary state is established. This means that the hydration process with $\tau_{hydrate}$ can bypass all other processes in a two-step transfer. The fact that two distinct values $\tau_1$ and $\tau_2$ are associated with the water exchange implies that $\tau_{hydrate}$ cannot be identified with the fast process $\tau_1$, as a fast bypass would mask the slower direct transfers.

Only two possibilities remain. Either the slow process $\tau_2$ represents the exchange between bound and free water, or it refers to a yet unidentified process while the exchange with free water is too slow to be observable. The second possibility can be excluded, as no free water peak can be detected, nor is any excessive line broadening observed. This leads to the conclusion that the exchange between free and bound water proceeds with the time constant $\tau_{hydrate} = \tau_2 = 35$ μs. It is worth noting that this value is considerably longer than the usual residence times reported for protein hydration water molecules in aque-

ous solution. For example, the estimated residence times for the surface hydration water molecules of BPTI at 279 K are ≤ 500 ps (Otting et al., 1991). Residence times between 100 ns and 1 μs have recently been reported for the four internally bound water molecules of BPTI by Denisov and Halle (1995a,b).

While the value $\tau_{hydrate} = 35$ μs can hardly be disputed, the interpretation of the measured product $p_A p_B \Delta^2 = 7225\ Hz^2$ of Eq. 8 causes difficulties. When $p_A$ and $p_B$ are identified with $p_{bound} = 0.82$ and $p_{free} = 0.18$ and $\Delta$ with $\nu_o(\delta_{bound} - \delta_{free}) = 852$ Hz, one calculates a product $p_{bound}p_{free}\nu_o^2(\delta_{bound} - \delta_{free})^2 = 107143\ Hz^2$ and is faced with a discrepancy by a factor of ≈ 15. The contradiction could stem from incorrect assumptions either about the relative populations of the free and bound water, or about the corresponding chemical shifts. One might postulate that the solubility of water in chloroform at 250 K is lower than that reported by Gibby and Hall (1931) by a factor of 18. However, a careful solubility study of water in chloroform at various temperatures, performed by T. Schulte-Herbrüggen (personal communication, 1995) using 1D proton NMR, rules out this possibility. One might consider the possibility that the chemical shift of free water in antamanide solution differs from the value obtained in a sample containing water and chloroform alone. For example, the chemical shift of the free water might be sensitive to tiny amounts of hydrochloric acid present in chloroform. Such amounts would not be exactly reproducible from sample to sample, leading to different values of $\Delta = \nu_o(\delta_{bound} - \delta_{free})$. Alternatively, a smaller value for $\Delta$ could occur if antamanide-bound peripheral water molecules exist that exchange rapidly with the free water molecules. In contrast to water molecules binding within the peptide ring, these water molecules would form short-lived hydrogen bonds and induce a downfield shift of the water resonance relative to the free water resonance. However, these arguments are purely speculative.

The rapid $T_1$-relaxation-active process $\tau_1$ must then refer either to the inter-site water exchange dynamics with $\tau_{site}$ or to the local bound-water dynamics with $\tau_{local}$. A distinction between the two processes and their detailed characterization is not possible based on the available NMR data. It is worth noting here that very rapid water exchange processes have been found for proteins in aqueous solution. For example, the water residence times in BPTI are significantly shorter than the rotational correlation time $\tau_{rot} \approx 8$ ns at 279 K (Otting et al., 1991). In the BPTI studies, the presence of negative NOE and ROE cross peaks at 279 K necessitated a model in which translational diffusion of water molecules to and from the protein surface dominates the intermolecular dipolar cross-relaxation. It is thus reasonable to expect a site-to-site exchange process within antamanide to be much faster than the exchange between bound and free water in chloroform solution. We note, however, that the absence of water-site exchange in the MD simulations (e.g. simulations iii and iv) suggests that $\tau_1$ refers instead to the local dynamics of the bound water, leading to the assignment $\tau_1 \approx \tau_{local}$.

*Comparison of NMR results with the MD simulations*

The antamanide–water system experiences conformational dynamics on the microsecond time scale and the NMR data refer to an average over interconverting conformers. In contrast, the time scale of the MD simulations is such that interconversion between conformers rarely occurs. Thus, one cannot expect detailed agreement between the experimental NMR parameters and those calculated from a single simulation trajectory. The situation is somewhat improved, however, when one considers the results from the set of MD simulations. As seen above, the various simulations permit the sampling of several low-energy conformations of antamanide, which are otherwise inaccessible within the time scale of a single trajectory. Analysis of the set of MD simulations suggests that water molecules can significantly influence the conformation of antamanide.

The various intermolecular hydrogen-bonding patterns, which compete with the intramolecular hydrogen bonds, provide a rationale for the observed changes in the NH chemical shifts induced by water. Similarly, the marked effect of the water molecules upon the backbone conformation of the peptide provides a basis for understanding the observed changes in the antamanide $H^\alpha$ and $C^\alpha$ chemical shifts upon addition of water, due to their dependence on the backbone dihedral angles $\Phi$ and $\Psi$ (Wishart et al., 1991; de Dios et al., 1993a,b). The simulations at 250 K show that the water molecules stay closely associated with antamanide for the duration of the simulation (400 to 1000 ps). This result is consistent with the $R_{1\rho}(H)$ data, which suggest water molecule residence times in the microseconds.

Hydration sites consistent with the observed water–$H^N$ NOEs can be identified by looking for water protons within 4 Å distance of the antamanide $H^N$ protons in the conformations provided by the simulations. For example, an analysis of water proton to $H^N$ distances in the final conformation of the single-water simulation with water molecule 13 (Fig. 8d) shows that the strongest NOE cross peaks would be expected to $Phe^6$ $H^N$ and $Val^1$ $H^N$, and a less intense cross peak to $Phe^{10}$ $H^N$. The weakest NOE would be expected to $Ala^4$ $H^N$. This relative order of the NOE cross-peak intensities is also seen in the NOESY experiments. The NOE between water and $Ala^4$ $H^N$ could be enhanced by a water molecule located at the site occupied by water molecule 12, seen in the final configuration from the corresponding single-water simulation in Fig. 8c. The two-water simulation (with water molecules 12 and 13) essentially superimposes the results of the two single-water simulations.

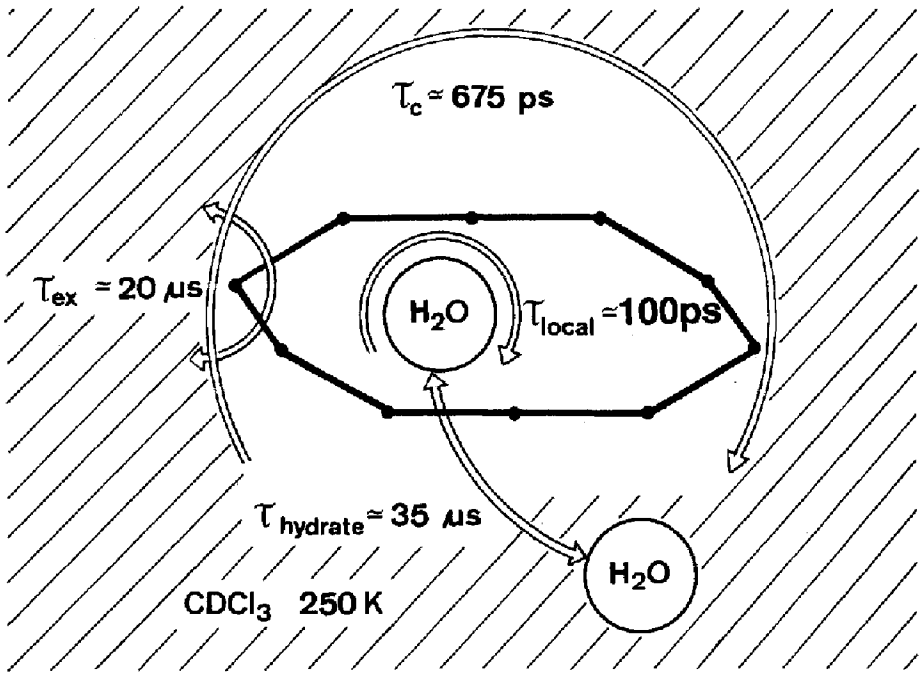


Fig. 12. Dynamic model of water interaction with antamanide in chloroform solution, together with the approximate time constants determined at 250 K in the present work.

Many of the NOESY-derived distances for antamanide fall within the range of distances spanned by the average structures obtained from the simulations. Table S5 in the Supplementary Material provides a comparison of selected interproton distances from both the NOE data and the MD simulations. An example of consistency between the NOE data and the simulations is the fact that both approaches identify the NH protons of $Phe^6$ and $Val^1$ as favorable hydrogen-bonding sites for water. More specifically, the one- and two-water simulations show that a single water (water molecule 13 in the simulations) is simultaneously hydrogen-bonded to the $Phe^6$ and $Val^1$ $H^N$ protons, and leads to a highly stable conformation. In the NOESY experiments, the $Phe^6$ and $Val^6$ $H^N$ protons give the strongest cross peaks to water. Since there are on average only 1.5 water molecules complexed with each antamanide, the binding configurations suggested by the one- and two-water simulations may be relevant.

The simulations further suggest that water molecules compete with the side-chain moieties of $Phe^9$ and $Ala^4$ for proximity above the plane of the antamanide ring. Water molecules force the phenyl rings away from the peptide ring in the fully hydrated simulation and in the one- and two-water simulations, where $Phe^6$ $H^N$ and $Val^1$ $H^N$ are bridged by a doubly hydrogen-bonded water molecule. This behavior is in accord with the NOE distances, which show an increase in the distance $Ala^4$ $H^\beta$-$Phe^9$ $H^\beta$ in the water-containing sample relative to the water-free sample. Additionally, the small decreases of backbone sequential $H^\alpha$-$H^N$ distances observed in the NOE analysis could be explained by a slight preference for the averaged conformations seen in the fully hydrated simulation and in the one- and two-water simulations. Comparison of the sequential $H^\alpha$-$H^N$ distances in the fully hydrated average structure with those from the water-free simulation reveals typically larger distances. This is a consequence of the more compact average structure seen in the water-free simulation.

The NMR $R_{1\rho}(H)$ and $R_2(C^\alpha)$ relaxation experiments suggest increased flexibility of antamanide in the absence of water molecules. The change in flexibility is especially evident for the peptide backbone region including $Ala^4$, $Phe^5$ and $Phe^6$. Corroborating evidence for these microsecond dynamics is not directly present in the simulations. While the water-free simulation does show somewhat enhanced rms fluctuations and flipping of the peptide planes between residues 3 and 4, it is unlikely that these motions reflect the dynamic processes sensed by the NMR $R_{1\rho}$ relaxation measurements, which operate on time scales up to microseconds.

## Conclusions

The aim of this study has been to characterize the interaction between the ion-carrier antamanide and water in the model lipophilic environment chloroform, through the combined use of NMR and MD simulations. The 250 K NOESY data show water molecules in close proximity to the antamanide backbone $H^N$ protons. The favored hydration sites are $Phe^6$ $H^N$ and $Val^1$ $H^N$. Water-binding conformations consistent with this observation have also been revealed in the MD simulations. The simulations

have demonstrated the higher stability gained by the presence of a water molecule acting as a cross-ring hydrogen-bonding bridge between the $Phe^6$ and $Val^1$ $H^N$ protons. The behavior of water as a cross-ring bridge is also consistent with the earlier crystal-structure determination by Karle et al. (1979).

Intermolecular cross-relaxation measurements provide evidence that water experiences local dynamics on a 100 ps time scale, without leaving the antamanide molecule (see Fig. 12). Bending and rotational modes of bound water, as well as rearrangements of the hydrogen-bonding network might be involved. On the other hand, $R_2$ and $R_{1\rho}$ measurements show that the exchange with free water in chloroform solution occurs on a 35 μs time scale. This mimics the water-binding properties of peptides in lipophilic media, such as in cell membranes, and thus provides insight into these properties. These techniques could also provide new possibilities for studying the detailed interaction of water with biomolecules by using a suitable nonaqueous solvent, such as chloroform.

The relaxation studies show that water-free antamanide experiences considerable backbone dynamics with characteristic time constants in the range 14–27 μs at 250 K. Water apparently reduces this flexibility, as suggested by the reduction of the transverse relaxation rate constants $R_2(C^\alpha)$ and $R_{1\rho}(H)$ in the water-containing sample. The cross-ring binding of water in the interior of the antamanide ring enhances the rigidity of the peptide backbone. In principle, it cannot be completely ruled out that the reduction of the transverse relaxation rate constants is caused by water-induced chemical shift degeneracies, as opposed to a dynamical change. However, it seems unlikely that the presence of water could simultaneously reduce the chemical shift spread of $H^N$, $H^\alpha$, and $C^\alpha$ nuclei without affecting the conformation or the dynamics of the molecule. Thus, the interpretation of the reduced transverse relaxation rate constants as caused by hindered backbone dynamics of antamanide due to water seems more probable. The sensitivity of the conformational dynamics of antamanide to the presence of water may have implications for those interested in designing drugs which must pass between hydrophilic environments via a lipophilic barrier. Indeed, the drug design principles concerned with drug delivery and clearance could be expanded to include the possibility of changes in both the conformation and flexibility of a given candidate drug, depending on the water content of its immediate environment.

Unlike the $R_2$ and $R_{1\rho}$ relaxation data, the NOESY spectra do not reveal large differences between the water-free and water-containing samples. A detailed multiconformational analysis of the NOE data for the two antamanide samples has not yet been performed. Nonetheless, a comparison of $^{13}C^\alpha$, $H^N$, and $H^\alpha$ chemical shifts suggests that the conformational equilibrium of antamanide is somewhat altered by the presence of water. Moreover, the MD simulations also suggest that water can affect the conformation of antamanide. This is indicated by the sensitivity of the simulated structures to the initial location and number of the water molecules, and is epitomized by a comparison of the water-free and fully hydrated conformations. In fact, the simulations also suggest that a combination of antamanide with only one or two water molecules would result in an ensemble of conformations that would contain conformational aspects of both the water-free and fully hydrated antamanide. Such conformations would interconvert rapidly on the NMR time scale, and thus the NOESY spectra from the water-free and water-containing samples (with only 1.5 water molecules per antamanide) would not be expected to show large differences. It is conceivable that further agreement between simulation and experiment would be attained if a larger number of low-energy configurations could be generated. Multiconformational searching procedures, such as MEDUSA (Brüschweiler et al., 1991), could be expanded to encompass also intermolecular interactions, thereby generating larger ensembles of binding configurations that can subsequently be compared with experiment.

## Acknowledgements

The authors are very grateful to Prof. H.H. Limbach and co-workers for assistance with the antamanide sample preparations. We would like to acknowledge helpful comments by Dr. R. Brüschweiler. We also thank Dr. T. Schulte-Herbrüggen for useful discussions and for a detailed water–chloroform solubility study. J.W.P. was supported in part by Fellowship DRG of the Cancer Research Fund of the Damon Runyon-Walter Winchell Foundation. This research has been supported by the Swiss National Science Foundation.

## References

Abragam, A. (1961) *Principles of Nuclear Magnetism*, Clarendon Press, Oxford, U.K.

Berendsen, H.J.C., Postma, J.P.M., van Gunsteren, W.F., DiNola, A. and Haak, J.R. (1984) *J. Chem. Phys.*, **91**, 3684–3690.

Berendsen, H.J.C., Grigera, J.R. and Straatsma, T.P. (1987) *J. Phys. Chem.*, **91**, 6269–6271.

Blackledge, M.J., Brüschweiler, R., Griesinger, C., Schmidt, J.M., Xu, P. and Ernst, R.R. (1993) *Biochemistry*, **32**, 10960–10974.

Bloom, M., Reeves, L.W. and Wells, E.J. (1965) *J. Chem. Phys.*, **42**, 1615–1624.

Bothner-By, A.A., Stephens, R.L., Lee, J., Warren, C.D. and Jeanloz, R.W. (1984) *J. Am. Chem. Soc.*, **106**, 811–813.

Boyd, J., Hommel, U. and Campbell, I.D. (1990) *Chem. Phys. Lett.*, **175**, 477–482.

Bremi, T., Ernst, M. and Ernst, R.R. (1994) *J. Phys. Chem.*, **98**, 9322–9334.

Brunne, R.M., van Gunsteren, W.F., Brüschweiler, R. and Ernst, R.R. (1993) *J. Am. Chem. Soc.*, **115**, 4764–4768.

Brüschweiler, R., Blackledge, M. and Ernst, R.R. (1991) *J. Biomol. NMR*, **1**, 3–11.
Brüschweiler, R., Roux, B., Blackledge, M.J., Griesinger, C., Karplus, M. and Ernst, R.R. (1992) *J. Am. Chem. Soc.*, **114**, 2289–2302.
Burgermeister, W., Wieland, T. and Winkler, R. (1974) *Eur. J. Biochem.*, **44**, 311–316.
Carr, H.Y. and Purcell, E.M. (1954) *Phys. Rev.*, **94**, 630–638.
de Dios, A.C., Pearson, J.G. and Oldfield, E. (1993a) *Science*, **260**, 1491–1496.
de Dios, A.C., Pearson, J.G. and Oldfield, E. (1993b) *J. Am. Chem. Soc.*, **115**, 9768–9773.
Dellwo, M.J. and Wand, A.J. (1989) *J. Am. Chem. Soc.*, **111**, 4571–4578.
Denisov, V.P. and Halle, B. (1995a) *J. Mol. Biol.*, **245**, 682–697.
Denisov, V.P. and Halle, B. (1995b) *J. Mol. Biol.*, **245**, 698–709.
Deverell, C., Morgan, R.E. and Strange, J.H. (1970) *Mol. Phys.*, **18**, 553–559.
Dietz, W. and Heinzinger, K. (1984) *Ber. Buns. Phys. Chem.*, **88**, 543–546.
Dietz, W. and Heinzinger, K. (1985) *Ber. Buns. Phys. Chem.*, **89**, 968–977.
Doddrell, D.M., Pegg, D.T. and Bendall, M.R. (1982) *J. Magn. Reson.*, **85**, 323–327.
Ernst, R.R., Bodenhausen, G. and Wokaun, A. (1987) *Principles of NMR in One and Two Dimensions*, Clarendon Press, Oxford, U.K.
Gibby, C.W. and Hall, J. (1931) *J. Chem. Soc.*, 691–693.
Janes, N., Ganapathy, S. and Oldfield, E. (1983) *J. Magn. Reson.*, **54**, 111–121.
Kamath, U. and Shriver, J.W. (1989) *J. Biol. Chem.*, **10**, 5586–5592.
Karle, I.L., Wieland, T., Schermer, D. and Ottenheym, H.C.J. (1979) *Proc. Natl. Acad. Sci. USA*, **76**, 1532–1536.
Kay, L.E., Jue, T.L., Bangerter, B. and Demou, P.C. (1987) *J. Magn. Reson.*, **73**, 558–564.
Kay, L.E., Torchia, D.A. and Bax, A. (1989) *Biochemistry*, **28**, 8972–8979.
Kay, L.E., Nicholson, L.K., Delaglio, F., Bax, A. and Torchia, D.A. (1992) *J. Magn. Reson.*, **97**, 359–375.
Kessler, H., Griesinger, C., Lautz, J., Müller, A., van Gunsteren, W.F. and Berendsen, H.J.C. (1988) *J. Am. Chem. Soc.*, **110**, 3393–3396.
Kumar, A., Wagner, G., Ernst, R.R. and Wüthrich, K. (1981) *J. Am. Chem. Soc.*, **103**, 3654–3658.
Lipari, G. and Szabo, A. (1982a) *J. Am. Chem. Soc.*, **104**, 4546–4559.
Lipari, G. and Szabo, A. (1982b) *J. Am. Chem. Soc.*, **104**, 4559–4570.
Macura, S. and Ernst, R.R. (1980) *Mol. Phys.*, **41**, 95–117.
Mádi, Z., Griesinger, C. and Ernst, R.R. (1990) *J. Am. Chem. Soc.*, **112**, 2908–2914.
Marion, D. and Wüthrich, K. (1983) *Biochem. Biophys. Res. Commun.*, **113**, 967–974.
Mark, A.E., van Helden, S.P., Smith, P.E., Janssen, L.H.H. and van Gunsteren, W.F. (1994) *J. Am. Chem. Soc.*, **116**, 6293–6302.
Marquardt, D.W. (1963) *J. Soc. Ind. Appl. Math.*, **11**, 431–441.
Meiboom, S. and Gill, D. (1958) *Rev. Sci. Instrum.*, **29**, 688–691.
Naito, A., Ganapathy, S., Akasaka, K. and McDowell, C.A. (1981) *J. Chem. Phys.*, **74**, 3190–3197.
Naito, A., Ganapathy, S., Raghunathan, P. and McDowell, C.A. (1983) *J. Chem. Phys.*, **79**, 4173–4182.
Naito, A. and McDowell, C.A. (1983) *J. Chem. Phys.*, **81**, 4795–4803.
Nirmala, N.R. and Wagner, G. (1989) *J. Magn. Reson.*, **82**, 659–661.
Noggle, J.H. and Schirmer, R.E. (1971) *The Nuclear Overhauser Effect*, Academic Press, New York, NY, U.S.A.
Otting, G. and Wüthrich, K. (1989) *J. Am. Chem. Soc.*, **111**, 1871–1875.
Otting, G., Liepinsh, E. and Wüthrich, K. (1991) *Science*, **254**, 974–980.
Palmer III, A.G., Rance, M. and Wright, P.E. (1991) *J. Am. Chem. Soc.*, **113**, 4371–4380.
Palmer III, A.G., Skelton, N.J., Chazin, W.J., Wright, P.E. and Rance, M. (1992) *Mol. Phys.*, **75**, 699–711.
Pastore, A. and Saudek, V. (1990) *J. Magn. Reson.*, **90**, 165–176.
Patel, D.J. (1973) *Biochemistry*, **12**, 667–688.
Peng, J.W., Thanabal, V. and Wagner, G. (1991) *J. Magn. Reson.*, **95**, 421–427.
Press, W.H., Flannery, B.P., Teukolsky, S.A. and Vetterling, W.T. (1988) *Numerical Recipes in C – the Art of Scientific Computing*, Cambridge University Press, New York, NY, U.S.A., pp. 540–547.
Redfield, A.G. (1955) *Phys. Rev.*, **98**, 1787–1809.
Ryckaert, J.-P., Ciccotti, G. and Berendsen, H.J.C. (1977) *J. Comput. Phys.*, **23**, 327–341.
Schmidt, J.M., Brüschweiler, R., Ernst, R.R., Dunbrack, R.L., Josephs, D. and Karplus, M. (1993) *J. Am. Chem. Soc.*, **115**, 8747–8753.
Sklenář, V., Torchia, D. and Bax, A. (1987) *J. Magn. Reson.*, **73**, 375–379.
Spera, S. and Bax, A. (1991) *J. Am. Chem. Soc.*, **113**, 5490–5492.
Tironi, I.G. and van Gunsteren, W.F. (1994) *Mol. Phys.*, **83**, 381–403.
van Gunsteren, W.F. and Berendsen, H.J.C. (1987) *Groningen Molecular Simulation (GROMOS) Library Manual*, Biomos, Groningen, The Netherlands.
Wagner, G., Pardi, A. and Wüthrich, K. (1983) *J. Am. Chem. Soc.*, **105**, 5948–5949.
Wieland, T., Faulstich, H. and Burgermeister, W. (1972) *Biochem. Biophys. Res. Commun.*, **47**, 984–992.
Wieland, T. and Faulstich, H. (1978) *Crit. Rev. Biochem.*, **5**, 185–260.
Wishart, D.S., Sykes, B.D. and Richards, F.M. (1991) *J. Mol. Biol.*, **222**, 311–333.